THESIS FOR THE DEGREE OF DOCTOR OF PHILOSOPHY

IN THERMO AND FLUID DYNAMICS

Experimental evaluation of renewable drop-in fuel blends for compression ignition engines

JOSEFINE PREUß

Department of Mechanics and Maritime Sciences
CHALMERS UNIVERSITY OF TECHNOLOGY
Göteborg, Sweden 2021

Experimental evaluation of renewable drop-in fuel blends for compression ignition engines
JOSEFINE PREUß
ISBN 978-91-7905-530-1

Doktorsavhandlingar vid Chalmers tekniska högskola
Ny serie nr. 4997
ISSN 0346-718X

Department of Mechanics and Maritime Sciences
Division of Combustion and Propulsion Systems
Chalmers University of Technology
SE-412 96 Göteborg, Sweden
Phone: +46 (0)31-772 10 00

Chalmers Reproservice
Göteborg, 2021

Für Frida und Jonathan

Abstract

Driven by the need to reduce greenhouse gas emissions while meeting the growing demand for mobility, the transport sector is shifting towards more sustainable and less polluting energy sources. Although vehicle electrification is advancing, it will take decades for electric vehicles to completely replace all current vehicles powered by internal combustion engines. In the meantime, it may be possible to reduce the emissions originating from transport by replacing fossil Diesel fuel with renewable alternatives suitable for use in compression ignition combustion engines. Fuels that can be used in existing engines without modification of hardware or calibration settings are called drop-in fuels. The scientific contribution of this dissertation is an experimental evaluation of potential drop-in fuel blends for the use in a compression ignition engine.

The main component of each studied blend was either a long-chain alcohol or poly(oxymethylene) dimethyl ether (OME_{3-5}) blended with hydrotreated vegetable oil and rapeseed methyl ester as well as fossil Diesel fuel in some cases.

The performance and emissions of the different fuel blends were investigated experimentally in heavy duty and light duty single cylinder research engines. Some of the long-chain alcohol blends were also investigated in a heavy duty multicylinder engine as well as in optical spray experiments using a high-pressure/high-temperature constant volume chamber.

Overall, the obtained results indicate that blends consisting mainly of long-chain alcohols or OME_{3-5} could replace fossil Diesel fuel in compression ignition engines. Owing to the lower heating value of the fuel blends, the fuel consumption increases slightly. But there is the possibility of improved engine efficiency. Importantly, both long-chain alcohol and OME_{3-5} blends have the potential to greatly reduce soot emissions. It was concluded from optical spray studies that not only the oxygen content of the fuel but also the increased heat of evaporation influenced the combustion and thus the soot reduction potential.

However, light duty engine tests using these blends yielded strongly increased NO_x emissions, and the high particle number emissions observed in the heavy duty engine tests could be problematic given the limits on particulate emissions imposed by the most recent emissions standards.

Keywords*: Renewable fuels, Compression Ignition Engine, long-chain alcohol blends, OME_{3-5} blends, Particle emissions, NO_x emissions.*

Populärvetenskaplig sammanfattning

Experimentell utvärdering av förnybara bränsleblandningar för kompressionständningsmotorer

Världens befolkning ökar och därmed behovet av mobilitets- och transportlösningar. Utsläpp från vägtransporter (personbilar och lastbilar) bidrar till nästan en femtedel av de globala utsläppen av växthusgaser och bidrar till luftföroreningar i tätorter. Åtgärder för att minska utsläppen för att uppnå klimatmålen är bland annat förbättrad transportinfrastruktur, innovativa fordonstekniker samt användning av bränslen med låga utsläpp. Målet är en övergång till mobilitets- och transportlösningar utan utsläpp.

Trots att andelen hybrid- och helelektriska fordon ökar, kommer fordon med enbart förbränningsmotorer att dominera på vägarna under det kommande decenniet. I Europa har var fjärde personbil som säljs idag en dieselmotor samtidigt som nästan uteslutande alla tunga transporter också drivs av en dieselmotor. Fossil diesel utgör idag det vanligaste bränslet för dieselmotorer på både tunga och lätta fordon. Ett sätt att minska användandet av fossil diesel är att utveckla förnybara drop-in bränslen, vilket innebär att ingen ändring av motorhårdvaran är nödvändig. Forskning krävs dock för att identifiera effekten av dessa nya bränslen med avseende på motorns prestanda och utsläpp.

Denna avhandling utvärderar flera bränslekandidater för deras potential att användas i dieselmotorer i person- och lastbilar. Målet är att minska utsläppen jämfört med fossil diesel men med bibehållen prestanda. Bränsleblandningar som undersöktes i detta arbete bestod huvudsakligen av alkoholer eller ester tillsammans med kommersiellt tillgänglig förnybar vätebehandlad vegetabilisk olja. Blandningarna togs fram för att efterlikna egenskaperna hos fossilt dieselbränsle i syfte att underlätta möjligheten till drop-in. Experiment med singelcylindriga forskningsmotorer visade att bränsle som innehåller alkoholer eller ester kraftigt minskade utsläppen av sot samtidigt som motorns prestanda bibehölls. Nackdelar för användning i lätta fordon var de ökade utsläppen av kvävedioxider och för tunga, ökningen av små partiklar. Slutsatsen är att de testade bränslena har potential att ersätta fossil diesel.

List of Publications

This thesis is based on the following publications:

I. J. Preuß, K. Munch, I. Denbratt, "Performance and emissions of long-chain alcohols as drop-in fuels for heavy duty compression ignition engines," *Fuel*, vol. 216, pp. 890–897, 2018.

II. J. Preuss, K. Munch, M. Andersson, I. Denbratt, "Comparison of long-chain alcohol blends, HVO and Diesel on spray characteristics, ignition and soot formation," *SAE Technical Paper 2019-01-0018*, 2019.

III. J. Preuss, K. Munch, I. Denbratt, "Effect of injection strategy and EGR on particle emissions from a CI engine fueled with an oxygenated fuel blend and HVO," *SAE Technical Paper 2021-01-0560*, 2021.

IV. J. Preuß, K. Munch, I. Denbratt, "Performance and emissions of renewable blends with OME_{3-5} and HVO in heavy duty and light duty compression ignition engine," *Fuel*, vol. 303, 121275, 2021.

Other relevant publications co-authored by Josefine Preuß:

V. N. Sharma, J. Preuss, J. Sjöblom, "Morphological Characterization of Soot from Diesel and an oxygenated fuel from a Compression Ignition Engine," *in submission*, 2021.

Acknowledgements

A lot of things must improve to reduce the human footprint on our planet and I am grateful to do research on a small area to contribute to this important goal. Therefore I would like to thank my supervisors Ingemar Denbratt and Karin Munch for the opportunity to work in this exciting project. I learned a lot from the discussions I had with the both of you. Thanks for creating a good working atmosphere and for the exchange of ideas.

This work is part of the project 'Future alternative transportation fuels' funded by the Swedish Energy Agency, which I thank for the financial support.

I am grateful for the help I got with my experimental work from the lab engineers especially from Timothy Benham, Alf-Hugo Magnusson, Patrik Wåhlin, Robert Buadu, Anders Mattsson and Lars Jernqvist. Thank you for sharing your expertise with me. The help with the spray chamber tests from Chengjun Du and Mats Andersson was highly appreciated. Thank you Mats for patiently answering all my questions and Chengjun for guiding me through the optical set-up. Thank you Jonas Sjöblom for many interesting and inspiring discussions and thank you Nikhil Sharma for the great collaboration.

The project involved many people and I consider myself lucky that the cooperation was very adjuvant, productive and friendly. Thank you Maria Grahn, Nika Alemahdi, Sofia Poulikidou, Stefan Heyne and Tara Larsson. Also I am thanking Ulf Östan from Saybold for the support with the CN tests. Further I would like to acknowledge Fredrik Ekström, Monica Johansson, Per Hanarp and Golnar Azimi for their support with the engine tests.

That I have so helpful and funny colleagues at the division, made my work enjoyable. I would like to especially thank Lucien Koopmans, Elenor Norberg, Blagica Smilevska, Ulla Lindberg-Thieme, Erik Sjödin and Sven Andersson as well as former colleagues for creating a great working environment.

Finally, I like to thank my parents and my sister for their support as Anders and his family for their encouragement and interest in my work.

Josefine Preuß
Göteborg, August 27^{th}, 2021

Contents

Part I.

Introductory chapters

1. Introduction

1.1. Motivation

The ongoing transition from a fossil-based economy to a sustainable economy is being driven by the growing concern about and awareness of the anthropogenic greenhouse effect and the accompanying global warming. The transport sector accounted for 24 % of the world's total greenhouse gas (GHG) emissions in 2017, and three quarters of these emissions originated from road traffic [1].

Emissions from road traffic have strong negative effects on air quality, especially in urban areas, and cause several health and environmental problems. Engine exhaust contains several pollutants, including nitrogen oxides (NO_x), carbon monoxide (CO), unburned hydrocarbons (UHC), and volatile organic compounds that contribute to air pollution and thus adverse climatic effects. The release of NO_x, sulfur oxides, and ammonia into the atmosphere causes acidification of soils and waters. Most modern Diesel fuels therefore have a very low sulfur content or are sulfur-free. Particulate matter emissions from internal combustion engines also have negative effects on human health; in particular, they are linked to many respiratory problems [2].

Future scenarios for the European Union predict that existing measures will be insufficient to reduce GHG emissions (Figure 1.1) [3]. Therefore, at the end of 2020, the European Union decided to implement additional measures as part of the 'European green deal', with the goal of achieving carbon neutrality by 2050. Measures called for within this strategy include increasing the energy efficiency of transport systems, promoting low-emission transport using alternative and renewable fuels (biofuels, hydrogen, and renewable synthetic fuels), and transport electrification using low and zero emission vehicles.

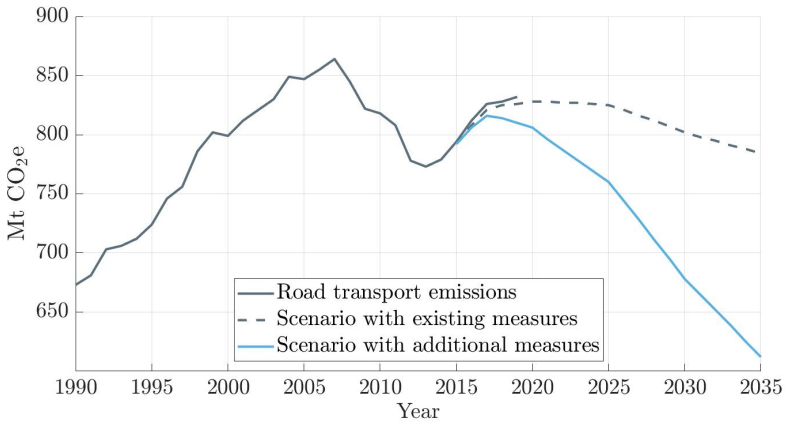

Figure 1.1.: Changes in GHG emissions from 1990 for road transport in the European Union (EU-27) (adapted from [3])

In 2020, the market shares of newly registered cars by fuel type in the EU were 28 % for Diesel, 47.5 % for petrol, 11.9 % for hybrids, 10.5 % for electric, and 2.1 % for alternative fuels. Most vehicles in the latter category are fueled with ethanol (E85), liquid petroleum gas, or natural gas [4]. In recent years, the market share of new Diesel and petrol vehicles has fallen slowly while that of vehicles with alternative powertrains has risen. Expected vehicle lifetimes vary widely and depend on the manufacturer and model. However the average lifespan of passenger cars in 2020 was around 17 and 18 years in Sweden and Germany, respectively, with an increasing trend [5, 6]. Therefore, existing petrol and Diesel-powered vehicles will not be removed from the roads for some time, making it necessary to introduce less polluting (non-fossil) fuels for these vehicles if climate goals are to be achieved.

To control the risks presented by exhaust emissions and reduce the danger they present to public health, many jurisdictions have introduced laws requiring vehicle manufacturers to reduce the emissions of their products. Table 1.1 shows the latest emission standards for light and heavy duty vehicles in Europe.

One way to help achieve compliance with these new emissions standards is to introduce fuels that are produced from sustainable resources and can be used in standard commercial engines without modifying the engines' hardware or calibration settings.

Table 1.1.: Emission limitations for light and heavy duty engine in Europe [7]

		Light duty	**Heavy duty**
Emission Standard		**Euro VI**	**Euro VI** (steady state testing)
Driving cycle		WLTC	WHSC
Year		2014	2013
CO	g/kWh	0.5	1.5
HC			0.13
HC + NO_x		0.17	
NO_x		0.08	0.4
PM		0.005	0.01
PN	1/kWh	$6 \cdot 10^{11}$	$8 \cdot 10^{11}$
NH3	ppm		0.01

Biodiesel and hydrotreated vegetable oil (HVO) are commercially available renewable alternative fuels for compression ignition engines. Biodiesel consists mainly of fatty acid esters produced by transesterifying vegetable oils. Neat biodiesel (B100) is used in some countries, but it requires engine modification. Alternatively, it can be blended with conventional Diesel fuels; in many European countries, fossil Diesel is routinely blended with up to 7 % of rapeseed methyl ester (RME), a biodiesel derived from rapeseed oil. Interest in HVO has risen over time because it promises significant reductions in emissions (e.g. [8, 9, 10]). HVO is produced by hydrotreating vegetable oils and animal fats. A life cycle assessment combining electrification (hybrid, plug-in hybrid and battery electric vehicle) and HVO revealed that the combination of a hybrid electric vehicle fueled with HVO promised a GHG reduction of 74 %, which exceeds the GHG reduction potential of a battery electric vehicle (when considering 2020 European electricity mix) [11].

Interest in the use of oxygenated alternative fuels such as alcohols and fatty acid esters is also increasing. Replacing fossil fuels with oxygen-containing alternatives could potentially reduce CO_2, CO, and soot emissions while maintaining engine performance [12, 13, 14, 15]. However, the use of renewable fuels also affects engine power and exhaust emissions, and can change the nature of the particulate matter in the exhaust. Further research on these fuels is therefore needed to find ways of reducing emissions without harming vehicle performance.

1.2. Objective

This work aimed to identify alternative fuels that could be used in compression ignition engines in the near future. Specifically, the objective was to identify fuels that can be produced renewably and used as drop-in replacements for fossil Diesel, meaning that they can be used in existing compression ignition (CI) engines without requiring any changes in the engines' hardware or calibration settings. Drop-in fuels must also be compatible with the materials used in existing engines, achieve cold starts without issue, and be compatible with established fuel distribution infrastructure.

The fuel components were chosen based on their potential to reduce well-to-wheel greenhouse gas emissions. A critical assessment from a life cycle and system perspective exceeds the scope of this work, but was performed within the framework of the project *'Future alternative transportation fuels'*.

To satisfy the requirements for drop-in fuels, blends were designed such that each of their components would compensate for one or more of the drawbacks of another component while preserving their advantages in terms of emissions reduction and engine performance. These blends were composed of vegetable oils (HVO, RME) blended with either long-chain alcohols or poly(oxymethylene) dimethyl ether (OME_{3-5}). The results presented herein enhance our understanding of the design of renewable alternative fuels and reveal potential challenges resulting from the use of such fuels in standard CI engines.

Long-chain alcohols are typically defined as alcohols with alkyl chains containing at least six carbon atoms. They are considered promising candidate drop-in fuels because of their high calorific value compared to short-chain alcohols such as ethanol (which has a carbon chain length of 2); the calorific value of alcohols increases with the carbon chain length. The carbon chain length is denoted C_n where n is the number of carbon atoms in the chain. This work focused on fuel blends featuring the C_8 alcohols n-octanol (Oc) and its isomer 2-ethylhexanol (2-EH), and the C_{10} alcohols n-decanol and its isomer 2-propylheptanol (PH). Experiments were performed using blends of these alcohols with HVO, fossil Diesel, and RME.
Further experiments were performed using blends of OME_{3-5} with HVO, RME, and various alcohols added to improve miscibility. Due to its favorable chemical compo-

sition and structure, OME_{3-5} has the potential to significantly reduce soot emissions without substantially increasing NO_xemissions.

The impact of the blend composition on engine performance and emissions was studied experimentally using a Volvo D13 single cylinder heavy duty research engine, which was operated using the D13 production engine's standard settings. Additionally, light duty engine tests, using a Ricardo hydra engine with a standard Volvo NED4-cylinder head were carried out. Deeper insights into the combustion behavior of selected fuel blends were obtained by performing optical experiments in a constant volume high-pressure/high-temperature chamber. A selected renewable fuel candidate was also tested in a heavy duty multi-cylinder engine with a state of the art aftertreatment system. Both the engine and spray experiments were designed to help answer the research questions listed below:

- Do blends containing long-chain alcohols or OME_{3-5} have the potential to be used as drop-in fuels in CI engines?
- How does the use of renewable fuel blends influence engine efficiency and fuel consumption?
- How large is the emissions reduction potential (for gaseous and particle emissions)?
- What are the challenges of using renewable fuel blends in CI engines?

2. Background

This chapter begins by briefly describing the properties, production, and usage of selected fuel candidates and blend components, i.e. rapeseed methyl ester and the reference fuels fossil Diesel and hydrotreated vegetable oil. In addition, the characteristics of the C_8 alcohols n-octanol and its isomer 2-ethylhexanol, the C_{10} alcohols n-decanol and its isomer 2-propylheptanol, and poly(oxymethylene) dimethyl ether are presented. Because the studied fuels were designed for use in CI engines, the formation of emissions in such engines is explained using a conceptual model of Diesel flame development. In addition, the formation of particulates during combustion is described in detail. Finally, the current state of the art in research on alternative fuels and their blends is summarized.

2.1. Fuel properties

Properties of the individual components of the studied fuel blends are presented in Table 2.1, along with the properties required for compliance with the EN 590 standard and the properties of fossil Diesel. The EN 590 standard defines the physical properties a fuel must possess to be sold in the EU and other European countries. All of the fuel components considered in this work have flash temperatures above $55°C$. As such, they comply with the EN 590 regulations and are classified as class 3 fuels. In addition, they are all immiscible with water and have low susceptibility to microbial growth, enabling their long-term storage and integration into the existing fuel supply infrastructure.

Fossil Diesel is used as reference fuel. The Diesel used in this study has a maximum sulfur content of 10 mg/kg and a maximum aromatic content of 8 % by mass. Sulfur can influence the performance of catalysts and indirectly contributes to soot agglomeration and aromatic compounds are known soot precursors [25]. Therefore, low levels of both are beneficial for reducing soot emissions.

Table 2.1.: Fuel properties [16, 17, 18, 19, 20, 21, 22, 23, 24]

		EN590	Diesel	HVO	RME	Long-chain alcohols				Ether
						n-Octanol	2-ethyl-hexanol	n-Decanol	2-propyl-heptanol	OME_{3-5}
Density	kg/m^3	820-845	830	779.9	883	830	832	829	832	1066.5
CN		51	52	75/87.8[1]	52.9	37.5	23.2	48.2	33.3	54.5
Flash point	$°C$	>55	74	<61	140	80	75	82	100	63
Lower heating value	MJ/kg		42.9	44.1	38	38.4	38.4	38.9	38.9	19.1
Oxygen content	%		-	-	10	12.3	12.3	10.3	10.3	43.1
Boiling point	$°C$		180-370	180-320	280-350	195	184	221.5	218	117-241
Kinetic viscosity, 40$°C$	mm^2/s	2-4.5	3.04	2.6	4.5	5.6	5.2	8.47	6.5	1.18
Latent heat of evaporation	kJ/kg		250			545	389	310		
Vapor pressure (25$°C$)	kPa		<1.2	0.09	0.42	0.02	0.03	0.001	0.002	
Molar weight	g/mol		166.3	187.9	322.5	130.2	130.2	158.3	158.3	160.2
$AFR_{stoich.}$	-		14.45	14.89	12.56	13.18	13.18	13.44	13.44	5.83
H/C	-		1.83	2.15	1.81	2.25	2.25	2.20	2.20	2.34
O/C	-		-	-	0.095	0.125	0.125	0.1	0.1	0.83

[1] HVO with higher CN used in heavy duty tests with long-chain alcohol blends.

Hydrotreated vegetable oil (HVO) is an aliphatic paraffinic hydrocarbon with properties similar to Diesel fuel. It can be produced from various feedstocks without greatly affecting the final product quality. The feedstock for the HVO consumed in Sweden (2019) consists mainly of oil from animal fat (45 %), palm fatty acid distillate (33 %), and palm oil (7 %) [26].

Use of HVO has increased markedly in recent years, and the global production volume in 2025 is forecast to be twice that in 2019 [27]. Possible feedstocks are oils and fats from waste, vegetable oils from crops such as rapeseed, sunflower or palm oil, as well as jatropha and algae [26, 28]. Feedstocks may vary between regions and suppliers but do not significantly affect the fuel's properties [9]. Depending on the feedstock used, the well-to-wheel GWP of HVO is at least 50% lower compared to fossil Diesel. Emissions originated from soil during the agricultural cultivation have a substantial part to the GWP of HVO. However, the energy demand was increased for HVO production [28, 29]. A life cycle assessment performed by Andersson and Börjesson [11] demonstrated, that GHG emissions can be reduced by 74 % when fueling a hybrid electric vehicle with HVO (considering 2020 European electricity mix). This exceeds the reduction potential of a battery electric vehicle. Moreover, in a predicted scenario for 2050, a hybrid electric

vehicle fueled with HVO still performed better than the battery electric vehicle in regard to GHG emission reduction.

HVO production involves an initial pretreatment process that removes impurities from the feedstock. The unsaturated fatty acid chains are then converted to less reactive oxygen-free saturated paraffinic alkanes via a two-stage hydrotreatment and isomerization process. Depending on the feedstock, the carbon chain length of HVO ranges from C_{15} - C_{18} [22]. HVO has the benefit of a high heating value and a cetane number (CN) above 70, is sulfur-free, and has a low aromatic content (< 1 % by mass). Its density is slightly lower than that of standard European Diesel fuel, and outside the range permitted by the EN 590 standard. However, its high heating value compensates for its low density. Its boiling point is lower than that of Diesel, and its boiling curve is less steep. Consequently, it can be used at temperatures as low as – $40°C$ [22].

Rapeseed methyl ether (RME) contains saturated and unsaturated fatty acids. It is produced by extracting rapeseed oil, refining it, and then transesterifying it with methanol. Its properties are similar to those of Diesel, although its density is slightly higher. It has already been integrated into the existing transportation fuel infrastructure and is blended with fossil Diesel (at levels of up to 7 % by mass in some EU countries) to reduce well-to-wheel CO_2 , CO, HC, and particulate emissions. Its effects on NO_x emissions depend on the engine design and manufacturer [23, 30, 31].

n-Octanol is used as synthetic intermediate in the production of surfactants, perfumes, and flavors. It can be prepared from fossil resources via the reaction of butadiene with water [32]. However, it has also been produced renewably on a lab scale via biosynthesis using the bacterium Escherichia coli [33, 34]. In addition, Julis and Leitner [35] demonstrated the production of n-octanol by the conversion of biomass-derived furfural and acetone.

2-Ethylhexanol (EH) can be produced in several ways including biomass fermentation with ethanol, biomass gasification (with syngas as an intermediate product), or acetone-butanol-ethanol fermentation of biomass. Poulikidou et al. [29] performed a life cycle analysis and investigated the global warming potential (GWP) of EH production via different pathways. This analysis, which was based on the ISO 14044 international

standard and the method specified in the European Renewable Energy Directive (RED), concluded that the GWP of 2-EH is comparable to that of HVO, and that production via syngas delivers the lowest overall GHG emissions.

n-Decanol is used as plasticizer, lubricant, and surfactant, and can be biosynthesized using *E. coli* like n-octanol. ***2-Propylheptanol*** is used as a plasticizer in the production of polyvinyl chloride and other materials, and also as a surfactant or synthetic lubricant. Its production processes are similar to those of 2-ethylhexanol.

The C_8- and C_{10}-alcohols have Diesel-like densities and boiling points at the lower end of the accepted range for Diesel. They all have lower CN values than Diesel, and because of their branched structures, EH and PH have lower CN values than their linear isomers. However, all long-chain alcohols have higher CNs than the short chain alcohols methanol and ethanol. Moreover, their lower heating values (LHV) are higher than those of the commercially used fuel ethanol (26.8 MJ/kg) [36]. The energy output per kilogram of fuel increases with the carbon chain length, but the molar percentage of oxygen decreases with increasing chain length. All of these alcohols have higher latent heats of evaporation (a measure of the amount of energy needed to induce the fuel to go from the liquid to the gaseous state) than Diesel fuel. They also have higher kinematic viscosities, which can cause problems during fuel injection and spray formation.

Poly(oxymethylene)dimethyl ether (OME$_n$) has the general chemical structure CH_2-O-(CH_2-O)$_n$-CH_3, where n is the number of oxymethylene units. In the literature, OME$_n$ is also referred to as PolyDME, POMDME or PODE$_n$. It was recently identified as a potentially attractive alternative to fossil Diesel fuel for use in CI engines because it has the potential to deliver lower soot emissions with similar or only slightly increased NO_x emissions, allowing the soot-NO_x trade off to be avoided. OME$_n$ can be produced from the platform chemical methanol via several pathways. One pathway involves converting methanol into formaldehyde by dehydrogenation and then converting the formaldehyde into the intermediates trioxide and methylal, which are then converted into OME$_n$. Another possibility is the direct conversion of formaldehyde into OME$_n$ without the formation of intermediates. Its production is described in detail elsewhere [37, 38]. The production costs of OME$_n$ depend strongly on the price (and production pathway) of methanol, but can be competitive with those of fossil Diesel fuel [37, 39].

Currently OME_n is mainly produced in China and refined (stripped from formaldehyde) in Europe [40]. OME_n itself is produced as a mixture with components of different chain length. Research suggests the use of OME with n= 3-5 is preferred over OME with n=1, because the use of OME_1 requires changes in engine hardware (see Section 2.3.3). However, the percentual share of each chain-length in the blend varies with the production batch. The composition of the different units strongly influences the miscibility (with for example HVO or fossil Diesel fuel).

2.2. Compression ignition engine

Compression ignition engines are highly efficient because they can use high compression ratios. Unfortunately, despite ongoing development efforts, the formation of soot and NO_x emissions remains problematic even in high performance CI engines. This section presents a conceptual model of the combustion process in a CI engine and discusses the formation of gaseous and particulate emissions as well as strategies for reducing the levels of these unwanted pollutants.

2.2.1. Conceptual model of a reacting Diesel jet

To help understand Diesel combustion, a conceptual model of a burning Diesel fuel jet under quasi-steady state conditions was developed by Dec [41] based on data from optical experiments. The model describes a free jet that does not impinge on other jets or the combustion chamber wall. The experimental conditions were chosen to be within the typical range of engine operation conditions. Figure 2.1 shows how the model describes the structure of the fuel jet and flame formed as the injected fuel leaves the nozzle. As hot air is entrained into the liquid fuel jet, the fuel is vaporized, forming a rich fuel-air mixture close to the liquid spray tip. In this region, where the equivalence ratio is three to five and temperatures are above 1600 K, soot formation is initiated by polycyclic aromatic hydrocarbons (PAH), which are known to be key soot precursors. Final oxidation of soot occurs in the diffusion flame on the periphery of the jet.
Using Dec's model as basis together with data obtained using various optical assessment methods, his co-workers including Siebers and Pickett developed additional models for predicting the jet ignition (which gives information about the ignition quality), liquid penetration length and angle, and lift-off length in a constant volume chamber. The liquid penetration length is the maximum length of the liquid fuel jet. It depends mainly on

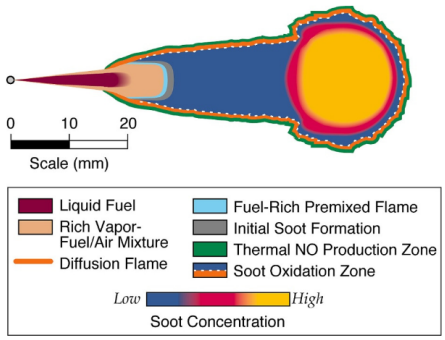

Figure 2.1.: Conceptual model of Diesel combustion [41]

the injector design and ambient gas conditions but is also affected by the fuel's properties [42, 43, 44]. The lift-off length is the distance between the nozzle and the first appearance of combustion downstream of the liquid jet. It is an important quantity because air and fuel premix in the lift-off region, and initial soot formation depends strongly on the composition of the air-fuel mixture. Lift-off length increases with decreasing ambient density and temperature or increasing injection velocity. The injection velocity can be increased by increasing the injector pressure or (to a lesser extent) the nozzle orifice diameter. A higher lift-off length results in a reduced equivalence ratio, a more homogeneous mixture, and lower soot formation [45]. When the equivalence ratio is < 2 at lift-off, soot-free combustion can be achieved [42]. The degree of premixing is also influenced by the fuel's CN: high CN fuels ignite faster, leading to shorter lift-off lengths and fuel-rich combustion [45]. Further details on soot formation can be found in Section 2.2.2.

Nitrogen oxide (NO) forms in the lean regions of the diffusion flame by the oxidation of atmospheric nitrogen. At high temperatures, NO can react with HO_2 to form nitrogen dioxide (NO_2). The term NO_x refers to the summed NO and NO_2 emissions, although NO levels are generally much higher. Higher flame temperatures during combustion lead directly to higher NO_x emissions[46]. NO_x emissions can be reduced by exhaust gas recirculation (EGR), in which some of the exhaust gas is fed into the intake manifold. This increases the heat capacity of the gas entering the cylinder, which reduces the combustion temperature and thus NO_x emissions. However, lower temperatures also reduce soot oxidation, resulting in a trade-off known as the Diesel dilemma [47, 48].

Models of soot formation in the fuel-rich region have also been developed by authors such as Kosaka et al. [49]. According to their model, particles coagulate and thus increase in size while moving downstream. Head vortices move the growing soot particles from the spray tip to the spray periphery, where the soot is oxidized. Unlike Dec's model, this model allows the liquid penetration length to exceed the lift-off length.

2.2.2. Particle emissions

Soot is produced by the incomplete combustion of hydrocarbon fuels. The total soot mass is determined by the competing processes of soot formation and soot oxidation. Simplistically, soot particle formation can be understood in terms of the five-step process as shown in Figure 2.2. In this process, the homogeneous nucleation of particles is followed by their coagulation into nuclei that then coagulate and grow into primary particle clusters through particle surface reactions. The primary particles then agglomerate. The rate of formation of soot precursors in the first step is low compared to the rates of nucleation and surface growth, so overall soot emissions depend strongly on the initial formation of soot precursors. The rate of soot precursor formation correlates with the number of carbon-carbon bonds in the fuel molecules, which can be related to the fuel's C/H ratio: as the C/H ratio increases, the fuel's sooting tendency decreases [25, 50].

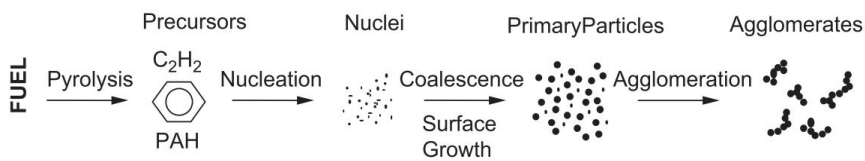

Figure 2.2.: Pathway of soot formation [25]

In the early 90s, Frenklach and Wang [51] proposed the HACA (H-abstraction-C_2H_2-addition) mechanism of soot formation. As the name suggests, the first step of this mechanism is the abstraction of a hydrogen atom from a reactive hydrocarbon. This is followed by the attachment of a gaseous acetylene molecule (C_2H_2) to the free vacancy. More recent research by Johansson et al. [52] suggests a clustering of hydrocarbons by radical-chain reactions with acetylene or vinyl groups. Both mechanisms thus involve the formation of covalent bonds between radicals and unsaturated hydrocarbons.

Soot oxidation occurs at temperatures above 1300 K throughout the combustion process [50], causing the soot to be converted into CO, CO_2, and H_2O. Oxidation is mostly driven by hydroxyl radicals (OH) and oxygen under lean conditions. Under stoichiometric and fuel-rich conditions, soot oxidation is mainly driven by OH.

The use of advanced fuels changes the nature of the particles that are formed. Additionally, the introduction of improved measurement systems has drawn greater attention to small particles whose size allows them to infiltrate the human body more readily than larger ones and also makes them more difficult to capture in aftertreatment systems. Soot emissions have been shown to contribute significantly to air pollution, causing human health problems and affecting global climate change [53, 54]. Procedures for capturing particles are based on the Particle Measurement Programme (PMP), which established standard methods for measuring and analyzing particle size distributions. The lower limit on particle size for particle number counting was set at 23 nm, mainly because of the limitations of the measurement technology available when the PMP was drawn up [55]. However, subsequent technological advancements have enabled the reliable detection and counting of smaller particles, so the cut-off size will probably be reduced to 10 nm in the future [53].

In the literature, particles are categorized according to their diameter: coarse mode particles have diameters above 500 nm, accumulation mode particles have diameters of 20-500 nm, and nucleation mode particles have diameters of 3-30 nm. Accumulation mode particles consist mainly of agglomerated and absorbed carbonaceous material while nucleation mode particles consist of volatile organic and sulfur compounds. Nucleation mode particles account for only 10 % of the total particle mass but over 90 % of the total particle number. Accumulation and coarse mode particles thus account for most of the emitted particulate mass. Figure 2.3 shows a typical exhaust particle size distribution [56]. In addition to the fuel's stoichiometry, the engine's operating parameters strongly affect the PSD. Particle mass emissions can be reduced by using higher injection pressures or earlier injection. As noted above, higher injection pressures lead to greater lift-off lengths and increased air entrainment, resulting in improved fuel-air mixing and the formation of leaner mixtures. Leaner conditions upstream also reduce emissions of unburned hydrocarbons, and the resulting higher peak temperatures promote soot oxidation [13, 57].

Zhang and Kook [58] identified a relationship between the injection timing and particle number emissions: retarding the injection of Diesel fuel in an optical engine from

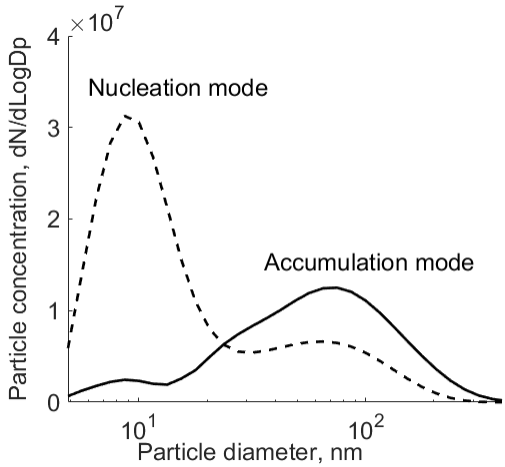

Figure 2.3.: Typical exhaust particle size distribution (adapted from [56])

-12 to -2 CAD ATDC caused an 80 % reduction in the particle number determined by analysis of TEM images. However, the change in injection timing had no apparent effect on primary particle sizes. Additionally, advancing the start of injection or raising the injection pressure reduces the diameters of primary soot particles and thus decreases soot formation, while the use of EGR leads to larger primary soot particles due to the lower in-cylinder temperature [59, 60].

The formation of nucleation mode particles is also influenced by dilution and the temperature in the tailpipe: fast cooling and a low initial concentration of precursors (and thus soot) favor the formation of nucleation mode particles, whereas a high initial concentration of agglomerated particles favors the adsorption of particles onto existing ones [61].

The processes of emission formation, including soot formation and oxidation, depend strongly on several factors and their interactions. These factors include physical parameters (temperature and pressure), the chemical composition of the fuel (e.g. its stoichiometry, structure, number of carbon-carbon bonds, H/C ratio, O/C ratio, and sulfur content), the properties of the fuel (e.g. its CN, density, volatility, heat of vaporization, heating value, boiling point), the engine's configuration (e.g. the combustion chamber geometry and the choice of injector system), and the engine's operating settings (load, EGR rate, injection pressure, injection duration, injection timing, and number of injections).

2.3. Renewable fuels in CI engines

Several strategies for reducing emissions from CI engines have been investigated, including optimization of fuel injection strategies (e.g. [60, 62, 63]), improving combustion system design to increase efficiency, and using alternative fuels. This chapter focuses on the effects of renewable fuels on combustion, with particular emphasis on results obtained using HVO, long-chain alcohol fuels and their blends, and OME fuels and their blends.

2.3.1. Hydrotreated vegetable oil

Interest in HVO has increased in recent years because of its Diesel-like properties which allow it to be blended with Diesel and used in most existing CI engines. Aatola et al. [64] and Hartikka et al. [9] found that both neat HVO and a blend of 30 % HVO in Diesel yielded lower emissions of CO, HC, NO_x and soot than neat Diesel when burned in a heavy duty DI engine with default injection timing settings. If the operating conditions were adjusted to maintain constant NO_x emissions, the HVO-containing fuels yielded even lower emissions and a lower specific fuel consumption. In addition, HVO-containing blends do not clog engines' aftertreatment systems, and their spray characteristics (penetration length, droplet size, and spray cone angle) closely resemble those of fossil Diesel. Lapuerta et al. [8] tested blends of HVO and ultra-low sulfur Diesel with HVO contents ranging from 10-75%, and found that the main factor limiting the usable percentage of HVO was its low lubricity. It was therefore recommended that the HVO content of HVO-Diesel blends should be capped at 50%. However, several car manufacturers permit the use of neat HVO with added lubrication in their engines.

2.3.2. Long-chain alcohols and their blends

The production of (bio)ethanol is increasing [26], and many researchers have investigated its use as a fuel or a component of blended fuels with fossil Diesel or gasoline (e.g. [14, 65, 66]). As mentioned previously, the key disadvantages of short chain alcohols such as ethanol are their low heating values and cetane numbers. Longer chain alcohols avoid these deficiencies because the heating value and cetane number increase with the carbon chain length. Blends of fossil Diesel and longer chain alcohols such as

butanol or pentanol have also been studied, revealing that they offer performance comparable to conventional Diesel with the benefit of reduced emissions due to their alcohol content [67, 68, 69]. However, this study focuses on alcohols with carbon chain lengths of eight and ten. The combustion of n-octanol and its isomers has been studied extensively, but that of n-decanol and its isomers has received less attention. Alcohols with carbon chain lengths above ten are not attractive fuels because of their high viscosity and the challenges of producing them on large scales.

Heuser et al. [70] tested neat n-octanol as a fuel in a single cylinder research engine, revealing that it produced similar NO_x emissions to Diesel with higher HC and CO emissions but significantly lower particulate emissions. Moreover, the engine's indicated efficiency was similar to that achieved with Diesel. These results were confirmed by 1D simulations and optical experiments using n-octanol in a high pressure chamber [71]. Further studies by Heuser et al. [72] compared neat n-octanol and its isomer, di-n-butyl ether (DNBE), to Diesel in a single cylinder research engine under five load conditions. The CN of n-octanol is lower than that of Diesel fuel whereas that of DNBE is higher. Consequently, their ignition delays (IDs) and combustion behaviors differed, leading to differences in the cylinder pressure and the rate of heat release. The EGR rate was adjusted in each case to keep NO_x emissions within the Euro VI limitations. The oxygen content of the fuels was 12.3 % by mass. Under these conditions, n-octanol yielded the lowest soot emissions but also the lowest indicated engine efficiency. Conversely, DNBE reduced soot emissions strongly without significantly reducing engine efficiency. PN emissions were measured with an Exhaust Emissions Particulate Sizer Spectrometer equipped with a thermal conditioner to remove volatiles. Both n-octanol and DNBE reduced PN emissions (relative to fossil Diesel fuel) for particles with diameters above 30 nm but increased those for particles below 30 nm.

Zhang et al. [73] evaluated the performance of a blend containing 30 % 2-ethylhexanol by volume in Diesel. Compared to conventional Diesel, this blend reduced particulate and CO emissions but slightly increased HC emissions at higher loads and had minor effects on NO_x emissions [69]. Later studies by the same group compared the performance of blends containing 30 % of either n-octanol or its isomer 2-EH by volume in Diesel and HVO in a single cylinder light duty CI engine. While all of these fuels delivered similar engine efficiencies, the PM and PN emissions achieved with the blends were lower than those for Diesel, but their NO_x emissions were slightly higher. Cold

start tests using a blend containing 30 % 2-EH, 40 % HVO, and 30 % Diesel by volume (giving an oxygen content of 3.8 % by mass) in a multicylinder engine showed that the blend remained ignitable at temperatures as low as –30 $°C$.

Wang et al. [74] studied blends containing 20 % and 40 % n-octanol in Diesel. The oxygen contents of these blends by mass were 2.5 % and 5 %, respectively. They were tested in a four-cylinder CI engine with a single injection, using injection pressures of 60-160 MPa under medium load conditions (1500 rpm and 0.8 MPa *bmep*, with a fixed start of injection). Compared to neat Diesel, the blends had a higher break specific fuel consumption (*bsfc*) and lower peak pressures but similar ignition delays and MFB50 values (representing the crank angle at which 50 % of the fuel is burned). Raising the injection pressure reduced CO and soot emissions, and the magnitude of this reduction was greater for the blends than for neat Diesel. NO_x emissions increased with the injection pressure, but soot PN emissions fell as the injection pressure increased until it reached 100 MPa. Above this threshold, further increases in the injection pressure caused no significant changes in PN emissions or the PSD.

Another study by the same group compared a Diesel/n-pentanol blend (D80P20) to a blend containing 64 % Diesel, 16 % n- pentanol, and 20 % DNBE by volume under the same medium load conditions. The EGR was varied from 0 % to 25 % in an attempt to find a combination of fuel and operating conditions that was optimal with respect to efficiency and emissions of soot and NO_x. The ignition delay, combustion duration, and *bsfc* all increased with the EGR rate. Efficiency was lowest for the Diesel-pentanol blend, and soot emissions decreased as the proportion of alcohol in the blend increased. Raising the EGR rate increased HC, CO, and soot emissions. The PSD revealed that large numbers of nucleation mode particles were emitted at EGR rates below 15 %, and that the blend with the highest alcohol content (and thus the highest oxygen content) produced the greatest number of particles in this size range [48]. In a similar study, Pan et al. [75] varied the EGR rate (0 % - 30 %) in a four-cylinder CI engine fueled with blends containing 20 % n-octanol and 40 % n-octanol in Diesel. In general, the ignition delay and combustion duration became shorter as the EGR rate was reduced because of the higher in-cylinder temperatures. At EGR rates below 15 %, the blends had higher thermal efficiencies than Diesel, but in other cases the efficiency was lower. CO emissions were generally lower for the blends and were similar for all EGR rates below < 20 %. Above this threshold, CO emissions increased strongly with the EGR rate for all fuels. NO_x emissions increased as the EGR rate decreased for all fuels. PN

emissions decreased strongly as the EGR rate decreased and the share of octanol in the blend increased. However, no strong shift to smaller particles was observed in this case. Nucleation mode particles were detected at all EGR rates below 20 %, but agglomeration mode PN emissions were consistently greater than nucleation mode PN emissions.

Simulations of n-octanol combustion have been performed to clarify its combustion behavior. Kerschgens et al. [76] used CFD based on the finite volume method to compare the combustion characteristics of n-octanol and its isomer DNBE, and validated their model against the results of experiments performed in an optical spray vessel under Diesel engine-like conditions. Differences in combustion performance and emissions were attributed to the ether group of DNBE, which gives it a higher CN than n-octanol, resulting in a shorter ignition delay. Bharti and Banerjee [77] performed reactive molecular dynamic simulations (ReaxFF MD) of n-octanol combustion at different equivalent ratios and temperatures, and found that major intermediates during n-octanol oxidation include formaldehyde and ethylene. The main drivers of the oxidation process were hydrogen absorption by molecular oxygen and the fraction of carbon-carbon double bonds in the fuel.

Optical studies in a high pressure/ high temperature (HP/HT) vessel were reported by Palmer et al. [78], who used Mie scattering and Schlieren imaging to study the liquid and vapor phases, respectively, of sprays formed from blends of n-octanol and DNBE under five different operating conditions. Increasing the content of n-octanol in the fuel spray led to reduced spray break up and slower evaporation, resulting in a longer liquid penetration length. The liquid penetration length depended linearly on the boiling temperature of the fuel. Zhang et al. studied the behavior of n-octanol and 2-EH sprays in a HP/HT chamber under non-combusting and combusting conditions. The alcohols had similar vapor phase properties to Diesel fuel, but their liquid phase characteristics depended strongly on their boiling point. Additionally, the CN was found to strongly affect the lift-off length. Longer lift-off lengths were associated with better fuel-air mixing and thus lower soot emissions. However, other factors including the fuel's latent heat of vaporization and volatility also affected the soot reduction potential of the blends [79].

Engine performance and emissions when using blends of n-decanol have been studied by only a few research groups. Janssen et al. [80] investigated the potential of n-decanol in a single cylinder research engine with EGR and found that it yielded 90 % lower particulate emissions than Diesel. 3D-CFD simulations supported this conclusion, indi-

cating that the higher heat of evaporation of n-decanol led to lower local temperatures in the reaction zone and thus lower soot formation. Moreover, soot was oxidized earlier in the combustion process when using the alcohol. Hottenbach et al. [81] studied n-decanol at four part-load points in a single cylinder research engine, and investigated spray characteristics in a HP/HT chamber. Compared to Diesel, n-decanol gave a higher ID, increasing the time available for air-fuel mixing and thus reducing soot emissions. The engine tests and optical tests complemented each other, and it was concluded that a shorter CN leads to a longer ID, and that this together with a high oxygen content favors low soot emissions.

In summary, replacing neat fossil Diesel with long-chain alcohols or blends of long-chain alcohols with either fossil Diesel or HVO can help reduce unwanted soot emissions from CI engines while minimizing increases in NO_x emissions. The reduction in soot emissions can be partly attributed to the blended fuel's higher oxygen content [14, 66, 73, 80, 82, 83]. However, a shift towards smaller particles was also observed under some operation conditions [74, 84, 85, 86, 87, 88]. The magnitudes of the reductions in soot emissions and the changes in the PSD depend strongly on operation conditions.

2.3.3. Poly (oxymethylene) dimethyl ether and their blends

Several studies have concluded that the combustion of OME_1 (also known as methylal or dimethoxymethane (DMM)) in CI engines is soot-free. However, OME_1 cannot be used as a drop-in fuel: modifications in engine hardware are required due to its high volatility, low flash point, and low lubricity [89, 90, 91, 92]. Blends containing OME with n>1 (specifically, mixtures of OME_n with n=3-5), are more likely to be compatible with existing engine technology. Therefore, research efforts have focused mainly on OME_{3-5} and higher molecular weight OME species.

Münz et al. [93] tested pure OME_{3-5} under real driving conditions (urban, rural and motorway) in an SUV-class vehicle equipped with a Diesel particulate filter [88]. Using a portable emission measurement system, the gaseous and particulate emissions generated using OME_{3-5} were compared to those for fossil Diesel fuel. The main injection duration and timing was changed to compensate for the reduced lower heating value (LHV) of OME_{3-5}. Particle number (PN) emissions were significantly lower than for Diesel and below the current legally mandated limit; even under urban driving conditions, OME_{3-5} reduced particulate emissions by around 60 % [88].

To investigate variations in combustion and emissions for different OME chain lengths,

Omari et al. [94] tested blends of 35 % OME_1 to OME_5 in Diesel. In general, changing the OME chain length had little effect on the results obtained; the indicated thermal efficiency when using OME was generally higher than for neat Diesel fuel, while HC, CO, and soot emissions were lower. It was concluded that the OME chain length should be chosen based on the ease of producing and using the different OME species since their combustion properties were so similar. Iannuzzi et al. [89] tested blends containing 5 % or 10 % by mass of OME_{2-6} in fossil Diesel in a single cylinder heavy-duty engine with a single injection strategy. Two load cases were examined while varying the EGR rate and SOI timing. Blends containing 10 % OME_{2-6} reduced soot emissions by up to 34 % but did not significantly affect NO_x emissions and thermal efficiencies. However, brake-specific fuel consumption was increased due to the low LHV of the blends. Dworschak et al. [95] investigated the performance, emissions, and PN of OME_{2-6} combustion in a heavy-duty CI engine under four load conditions without EGR. Compared to the reference fuel HVO, the indicated efficiency was higher and the combustion duration shorter for OME_{2-6}. The reduction of PN was load-dependent: the soot reduction potential was higher for lower load cases.

3. Experimental equipment and methods

3.1. Fuel blending strategy

To facilitate their use as drop-in fuels, the fuel blends were designed to mimic the properties of fossil Diesel, particularly its CN. The alcohols have relatively low CN, which is compensated for by the relatively high CN of HVO (see Table 2.1). Additional constraints for the design of the long-chain alcohol blends were that one blend should contain 20 % fossil Diesel, one should contain 10 % Diesel, and one should contain 7 % RME instead of Diesel. Finally, the content of HVO was not allowed to exceed 50 % by volume. The CN of n-decanol is comparable to that of fossil Diesel, so this fuel was not blended. The compositions of the designed blends are shown in Table 3.1 along with their oxygen content, density, LHV, and CN. The CN was determined by comparing the ignition performance (i.e. the ignition delay under given operating conditions with a predefined compression ratio) of the blend to that of a reference fuel, in accordance with EN ISO 5165 [96]. The test is designed for paraffinic Diesel fuels but can also be used for vegetable oils (e.g. HVO and fatty acid methyl ester fuels). However, there is no standard procedure for determining the CN of oxygenated fuels, so there is a relatively high degree of uncertainty in the blends' CN values . To ensure smooth injection, the alcohol-based fuels were supplemented with a lubricating additive at a concentration of 200 ppm per share of alcohol in the blend. The blends were named based on the abbreviations of their constituents (see Table 3.1) and their volumetric percentages in the blend. Another set of fuel blends containing OME_{3-5}, HVO, RME and 2-EH was also designed. At concentrations above 30 % by volume, OME_{3-5} did not mix with HVO at room temperature. Therefore, RME and the long-chain alcohol 2-EH were added, and the content of OME_{3-5} was kept below 30 %. The miscibility of OME_n depends strongly on the number of polyoxymethylene units in the polymer chain and the tem-

Table 3.1.: Composition and properties of designed long-chain alcohol blends

	Fuel	Diesel	HVO	RME	Ox	Density	LHV	CN
	vol.%	vol.%	vol.%	vol.%	m%	kg/m3	MJ/kg	-
References								
Diesel		100	-	-	-	830	43.16	52
HVO[1]	-		100	-	-	779.9	44.1	81
HVO		-	100	-	-	779.9	44.1	75
n-Octanol								
Oc47H33D20	47	20	33	-	5.9	813.5	41.12	52
Oc55H35D10	55	10	35	-	6.9	812.5	40.77	51,2
Oc58H35R7	58	-	35	7	6.7	816.2	40.28	49
2-Ethylhexanol								
EH36H44D20	36	20	44	-	4.6	808.7	41.74	51.9
EH45H45D10	45	10	45	-	5.7	808.4	41.34	52.3
EH43H50R7[2]	43	-	50	7	6.2	809.5	41.12	51.1
EH37H56R7	37	-	56	7	5.4	806.4	41.46	52.1
2-Propylheptanol								
PH46H34D20	46	20	34	-	4.8	813.9	41.41	52,4
PH55H35D10	55	10	35	-	5.7	813.6	41.05	50.9
PH58H35R7	58	-	35	7	6.7	817.3	40.57	49.3
n-Decanol								
Dec100	100	-	-	-	10.1	829	38.9	48.2

[1] HVO used only in HD single cylinder tests

[2] Blend contains HVO with higher CN (see Table 2.1)

perature. The OME_{3-5} mixture used to prepare these blends contained 0.3 % OME_2, 46.8 % OME_3, 29.2 % OME_4, 16.6 % OME_5 and 5.6 % OME_6 [24]. Basic compatibility experiments showed this mixture caused swelling of rubber parts and sealings: the mass of rubber seals increased by 55 % after being immersed in OME_{3-5} for 8 days. The mass of a pump membrane increased by 10 % under the same conditions. These observations are consistent with previous reports [91, 93, 97]. For example, Kass et al. [97] investigated the compatibility of OME-Diesel blends with elastomers and observed volume increases of up to 33 % in rubber components. They therefore concluded that either the rubber components of existing engines would have to be adapted to resist

OME_{3-5} blends or the content of OME_{3-5} in the blend would have to be relatively low. The addition of 7 % RME by volume is common in commercial Diesel fuels, and the share of EH in each blend was fixed at 10 % by volume. The blends and their densities, LHVs, oxygen contents, and cetane numbers are listed in Table 3.2. Lubrication oil was added all OME_{3-5} and long-chain alcohol blends at a concentration of 200 ppm per share of OME_{3-5} and 2-EH in the blend.

Table 3.2.: Properties of blends containing OME_{3-5}

	OME_{3-5} vol.%	**HVO** vol.%	**2-EH** vol.%	**RME** vol.%	**Ox** m%	**Density** kg/m^3	**LHV** MJ/kg	**CN** -
OME7H76	7	76	10	7	6.4	812.4	40.75	68.0
OME18H76	18	65	10	7	12.8	843.9	37.40	66.6
OME27H76	27	56	10	7	17.8	869.7	34.84	65.1

The densities of the blends were calculated linearly from the volume share of each component. The lower heating value for each blend was calculated from the heating values of each blend component and their mass fractions:

$$\mathrm{LHV}_{Blend} = \frac{1}{\rho_{\mathrm{Blend}}} \cdot \sum_{k}^{n} \rho_k V_k \mathrm{LHV}_k \tag{1}$$

Where *n* is the number of blend components *k* with density ρ_k, volume share V_k and lower heating value LHV_k.

3.2. Heavy duty single cylinder engine

Experiments were performed on a heavy duty compression ignition single cylinder research engine with a compression ratio of 17:1 and a cylinder head from a Volvo D13 engine. Table 3.3 shows the detailed engine specification.

Four load points adapted from the European Stationary Cycle (ESC) were used: A25, B50, B75 and C75. Here, B50 was deployed as a reference point, which was run at the beginning and end of each test cycle to evaluate the change in engine performance over time. Table 3.4 lists the engine parameters adapted from the factory settings. To investigate the influence of the fuel on combustion characteristics and emissions, all engine parameters were kept constant for all fuel blends as well as the Diesel reference.

Table 3.3.: Heavy duty CI engine specifications

Engine	AVL 501 single cylinder
Cylinder head type	Volvo D13
Displaced volume	2.13 dm^3
Bore	131 mm
Stroke	158 mm
Connecting rod length	267.5 mm
Compression ratio	17:1
Number of Valves	4
Fuel injection System	Common rail
Number of nozzles holes	5

However, with a lower heating value of the blends, the torque and *imep* was lower for the blends.

The fuel consumption was measured with as AVL 733S fuel balance. With a common rail F2 injector from Delphi, the fuel was injected in the combustion chamber. A pressure sensor (Kistler 7061B) and piezo amplifier (Kistler 3066A01) were used to measure cylinder pressure data, which were sampled with Osiris data acquisition software at a

Table 3.4.: Engine operating conditions

Operating conditions	**Unit**	**A25**	**B50**	**B75**	**C75**
Speed	r/min	1200	1500	1500	1800
Torque [1]	Nm	85	160	239	209
Imep[1]	MPa	0.61	1.10	1.59	1.41
Inj. time	BTDC	4.52	7.8	9.4	4.5
Inj. duration[1]	μ	668	1060	1466	1346
	CAD	4.8	9.5	13.2	14.5
Inj. pressure	bar	1800	1800	1800	1800
EGR	%	16.5	12.9	12.5	17.5
Boost pressure	mbar	1260	1936	2457	2726
Fuel flow	kg/h	2.39	5.14	7.37	8.17

[1] applies for operation with Diesel fuel

resolution of 0.1 CAD. The engine was equipped with an AVL554 oil cooling unit and AVL553 water cooling unit.

Exhaust gas emissions were measured using an AVL AMA i60 exhaust measurement system with the iGEM AMA software package. Nitrogen oxides were measured with a chemiluminescence system. This system works because nitrogen oxide formed during combustion reacts with ozone to form oxygen and an electronically excited nitrogen dioxide molecule, which emits a photon when it transitions to its ground state. The exhaust measurement system measures the intensity of the resulting light using a photodiode detector. A flame ionization detector (FID) was used to determine the concentration of unburned hydrocarbons in the exhaust by burning the hydrocarbons of exhaust samples in a hydrogen flame; this produces ions that are detected with a metal collector charged with a high DC voltage. The concentration of HC in the sample is directly proportional to the resulting current. Carbon monoxide and carbon dioxide were measured with infrared detectors; the concentration of each carbon oxide in an exhaust sample is proportional to the sample's infrared absorption at a specific wavelength. Each module of the exhaust gas analyser can achieve a full-scale reproducibility of 0.5 %. The exhaust gas recirculation (EGR) was regulated with a valve in the exhaust pipe and was calculated with the following equation.:

$$EGR, \% = \frac{CO_{2(\text{intake})} - CO_{2(atm)}}{CO_{2(\text{exhaust})} - CO_{2(atm)}} \cdot 100 \tag{2}$$

3.3. Heavy duty multi cylinder engine

Engine experiments in a 6-cylinder D13 engine were performed using fuel blend EH37H56R7 (short EHR7), which contains the long-chain alcohol 2-ethylhexanol, HVO, and RME (see Table 3.1). For comparative purposes, these experiments were also performed using the commercially available fuel B7 (93 % Diesel with at most 7 % fatty acid methyl ester by volume). This blend was chosen because its performance in the single cylinder heavy duty engine tests was similar to that of Diesel in all respects except that it yielded greatly reduced soot emissions. A key aim in this study was to evaluate its potential in a commercial engine.
The Volvo D13 engine is state of the art and complies with European Euro VI legislation. It has a maximum torque of 2600 Nm, a compression ratio of 18:1 and is equipped with a complete exhaust gas aftertreatment system including a selective catalytic reduction

(SCR) unit with a urea dosing system (UDS). Other engine specifications were the same as for the single cylinder engine (specification see Table 3.3).
The fuel B7 has a CN of 52, a density of 837 kg/m^3, a heating value of 42.6 MJ/kg and an oxygen content of 0.7 % by mass. Its heating value is thus 2.34 % higher than that of EHR7.
The multi-cylinder engine experiments used the ESC (see Figure 3.1), which has one load point representing idling at 550 rpm and 12 load points representing low, medium, and high load operation at three engine speeds
(1200 rpm, 1500 rpm, and 1800 rpm).

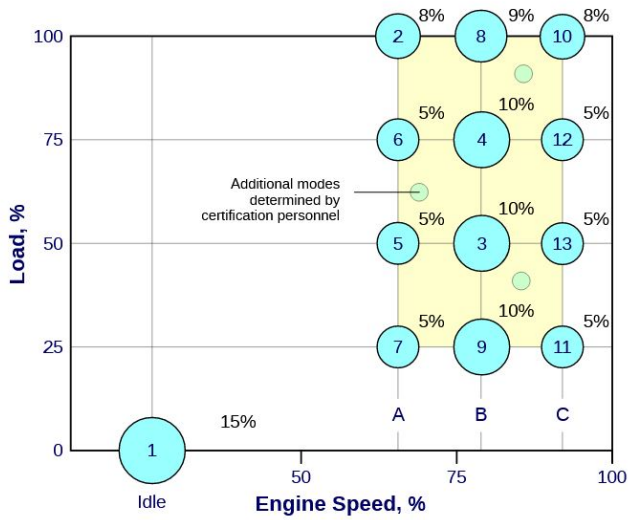

Figure 3.1.: European stationary cycle [7].

3.4. Light duty CI engine

Steady-state testing was carried out on a single cylinder light-duty Ricardo Hydra engine equipped with a Volvo NED4 cylinder head and a common rail injection system. Table 3.5 shows the engine specifications.
A Denso injector produced up to four pulse injections per cycle. Between the electrical signal of the injector and the actual injection of the fuel, injection rate measurements revealed a time delay of 0.24 ms, which corresponded to a delay of 1.8 CAD at 1280 rpm

Table 3.5.: Heavy duty CI engine specifications

Engine	Ricardo Hydra
Cylinder head type	Volvo NED4
Displaced volume	0.49 dm^3
Bore	82 mm
Stroke	93 mm
Compression ratio	15.8 : 1
Number of Valves	4
Fuel injection System	Common rail

[98]. This was accounted for in the analysis of the results.

Fuel mass flow was measured with an AVL 730 fuel balance. The in-cylinder pressure was measured using an AVL GUI2S-10 pressure transducer, amplified with a Kistler 5011 piezo charge amplifier and detected with an AVL IndiCom system. A resolution of 0.2 CAD was applied. NO_x emissions were measured with a Rosemount CLD 951A with an accuracy of <5 % of the full scale. A Rosemount Binos 1001/1004 Instrument measured the concentration of CO_2, intake and CO_2, exhaust with an accuracy of < 2 % of the full scale. EGR value was calculated based on the quotient of the carbon dioxide emission at the intake and exhaust (see equation 2).
Three load points were used, where load condition 1 was deployed as a reference point, which was run at the beginning and end of each test cycle to evaluate the change in engine performance over time. Table 3.6 lists the engine parameters adapted from the factory settings. To investigate the influence of the fuel on combustion characteristics and emissions, all engine parameters were kept constant for all fuel blends as well as the Diesel reference. A multi injection strategy (double-pre/main/post) was applied in these tests. The duration of all these four injections was increased for the blends to compensate for the lower heating value.

3.5. Particle measurement equipment

The particle mass per cubic meter of exhaust gas was measured with an AVL Micro Soot Sensor. This device uses photoacoustics to detect particle mass flow; the basic setup of

Table 3.6.: Engine operating conditions

Operating conditions	**Unit**	**1**	**2**	**3**
Speed	r/min	1280	1810	2000
Imep	MPa	0.88	0.74	1.12
Inj. pressure	MPa	79.3	66.9	91.1
EGR	%	19.1	27.3	22.5
Fuel flow[1]	kg/h	0.91	1.02	1.71

[1] applies for operation with Diesel fuel

the measuring unit is shown in Figure 3.2a. In this system, particles are exposed to modulated light. Upon heating, the particles expand, generating a sound wave that can be detected using microphones. The signal increases in proportion to the concentration of particles in the exhaust sample. The instrument's measuring range is 0.001-50 mg/m^3. To prevent condensation, the exhaust gas must be diluted with the integrated conditioning unit [99].
The particle size distribution in the exhaust was measured with a Cambustion DMS500 unit capable of detecting particles between 5 nm and 2.5 μm in diameter. In this instrument, the gas sample is passed through a corona charger that gives each incoming particle a positive charge proportional to its surface area. The charged particles then enter a classifier column (Figure 3.2b) where they are separated according to their charge and aerodynamic drag. An amplifier converts the resulting currents into data on particle numbers and sizes. The dilution factor was kept constant during the measurements because particle size measurements depend strongly on dilution [100]. Samples for both the Micro Soot Sensor and the DMS500 were taken at the exhaust tailpipe.

To remove volatile particles from the exhaust, a Dekati Thermodenuder (TC) was installed. Figure 3.3 shows its design and key components. In the thermodenuder, volatile organic compounds (VOC) are vaporized by heating the exhaust gas sample to 300 $^\circ C$ (573 K), after which the sample is cooled and passed over activated charcoal. This causes most hydrocarbon vapours to be adsorbed while particles pass unimpeded due to their different diffusion speeds. A flow rate of 10-20 L/min can be used [101]. However, pump limitations restricted the thermodenuder flow to 10 L/min.

A switch allows the measurement of particle numbers with and without volatile particle

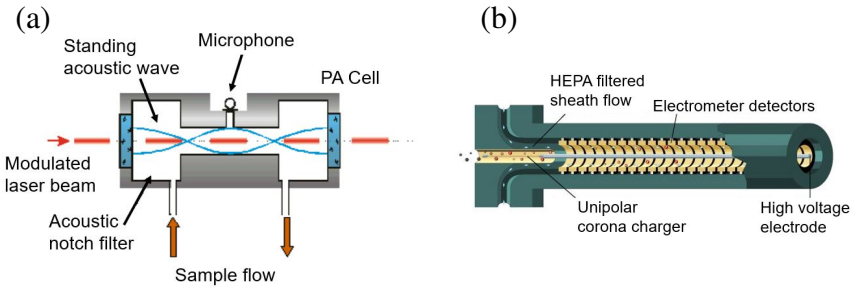

Figure 3.2.: (a) Design of a MicroSoot resonant cell. Image adapted from [99] , (b) Operating principles of the DMS500 particle size measurement system [100].

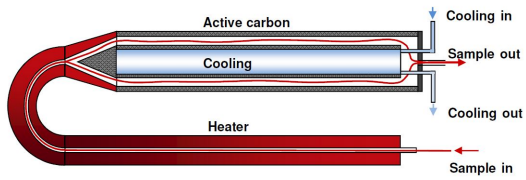

Figure 3.3.: Key components and flows in a thermodenuder [101].

removal. The capture efficiency of the thermodenuder over 38 size-bins was calculated as shown in equation 3 based on measurements obtained with and without the thermodenuder active.

$$\text{Capture efficiency} = \frac{PSD_{\text{raw}} - PSD_{TD}}{PSD_{raw}} \tag{3}$$

The capture efficiency was calculated when the difference in the particle counts obtained with and without the thermodenuder exceeded the combined standard deviation of the measurements. The measurement uncertainty was calculated as:

$$\varepsilon = t_{N-1.95\%} \sqrt{A^2 \cdot \text{var}(B) + B^2 \cdot \text{var}(A) + \text{var}(A) \cdot \text{var}(B)} \tag{4}$$

Here, $A = PSD_{raw} - PSD_{TD}$ and $B = PSD_{raw}^{-1}$ [102].

3.5.1. Combustion analysis

Indicated thermal efficiency

The indicated thermal efficiency η_t is the ratio of the work produced to the work and the work supplied to the system:

$$\eta_t = \frac{imep \cdot V_d}{\dot{m}_{Fuel} \cdot LHV} \tag{5}$$

Here, *imep* is the indicated mean effective pressure, V_d is the displacement volume of the engine, $\dot{m}_{fuel}$ is the mass flow of fuel and *LHV* is the fuel's lower heating value. The *imep* is calculated as the sum of the compression and expansion stroke work divided by the displacement volume and is thus a linear function of the cylinder pressure [46].

Indicated specific fuel consumption

The specific fuel consumption is the quotient of the fuel mass flow $\dot{m}_{fuel}$ and the obtained indicated power P_i.

$$\text{isfc} = \frac{\dot{m}_{Fuel}}{P_i} \tag{6}$$

Here, $P_i = \frac{imep \cdot V_d \cdot N}{n_R}$ and depends on the engine speed, N and the number of crank revolutions (n_R =2). Brake specific power P_b can be calculated in a similar way to the brake mean effective pressure (*bmep*).

Indicated specific emissions

Concentrations of engine out emissions (CO_2, CO, HC, NO_2, NO, O_2) were measured as volume percentages or in parts per million (ppm). Indicated specific emissions (isX) were calculated using equation 7, where *X* represents the emitted gas under consideration.

$$\text{isX} = \frac{u_x \cdot C_x \cdot \dot{m}_{\text{Exhaust}}}{P_i} \tag{7}$$

The ratio of the density of the gas and the exhaust is u_x, the measured concentration is C_x and $\dot{m}_{Exhaust}$ is the exhaust mass flow, which is the sum of the inlet air and fuel mass flows. For measurements using the light duty engine, a humidity correction factor was applied. Brake specific efficiency, fuel consumption and emissions can be calculated similarly, by dividing by the brake specific power P_b instead of P_i.

Coefficient of variation

The magnitude of cycle-to-cycle variation can be assessed using the coefficient of variation (COV) in *imep*, which can be computed using equation 8 [46]:

$$COV_{imep} = \frac{\sigma_{imep}}{imep \cdot 100} \tag{8}$$

The COV increases as the combustion becomes less stable. A COV below 3 % is required to ensure acceptably stable combustion.

Heat release analysis

The heat release analyses were based on the first law of thermodynamics [46]. As shown in equation 9, the chemical energy (dQ_{ch}) released by combustion was calculated as the sum of the change in the system's internal energy (dU_s), the piston work (dW), the heat transfer (dQ_{ht}), and the mass flow across the system boundaries per crank angle ($d\theta$). The system is regarded as stationary and a mass flow was neglected.

$$\frac{dQ}{d\theta} = \frac{dU}{d\theta} + \frac{dW}{d\theta} \tag{9}$$

Assuming ideal gas conditions in the combustion chamber, the internal energy and the work transfer can be calculated as follows:

$$\frac{dU}{d\theta} = mc_v dT \tag{10}$$

$$\frac{dW}{d\theta} = pdV \tag{11}$$

Here, m is the mass entering the system, c_v is the heat capacity at a specific volume, and p is the pressure. By combining equations 9–11 with the ideal gas law $pV=mRT$, where R is the ideal gas constant, T can be eliminated. Blow-by was neglected and the time frame for analysis was the period between inlet valve closure (θ_0) and exhaust valve opening (θ_{end}).

The Woschni correlation was used to estimate the convective heat transfer between the gases and the cylinder wall.

$$\frac{dQ_{ht}}{d\theta} = Ah_c\left(T - T_w\right) \tag{12}$$

Here, $h_c = 3.26 \cdot B^{-0.2}p^{0.8}w^{0.8}T^{-0.55}$ and depends on the bore (B), pressure (p), average cylinder gas velocity (w), and the temperature (T) [103].

By applying the ideal gas equation, the heat release per crank angle degree (dθ) was calculated as follows:

$$\frac{dQ_{ch}}{d\theta} = \left(\frac{c_v}{R}\right) \cdot V \cdot \frac{dp}{d\theta} + \left(1 + \frac{c_v}{R}\right) \cdot p \cdot \frac{dV}{d\theta} + Ah_c \left(T - T_w\right) \tag{13}$$

The mass fraction burned (MFB10, MFB50 and MFB90) awere calculated from the corresponding cumulative heat release, obtained by integrating equation 14 over the appropriate range of dθ.

$$Q_{ch} = \int_{\theta_0}^{\theta_{\text{end}}} \frac{dQ_{ch}}{d\theta} d\theta \tag{14}$$

In addition, the relative contributions of premixed and diffusion-controlled combustion were estimated from the heat release (dQ_{ch}) profile and its derivative (d^2Q_{ch}); the start of diffusion-controlled combustion was taken to coincide with a change in the slope of the heat release profile. For further details, see Paper III.

Air-fuel ratio

Lambda and the mass flow of air were determined from the exhaust gas composition. Therefore, the stoichiometric air-fuel ratio was derived from the equation for the stoichiometric (complete) combustion of an oxygenated fuel:

$$C_xH_yO_z + a \cdot (O_2 + 3.76 \cdot N_2) \rightarrow x \cdot \mathrm{CO_2} + \frac{y}{2} H_2 \cdot O + a \cdot 3.76\ \mathrm{N_2} \tag{15}$$

Based on this equation, a can be expressed as $a = x + \frac{y}{4} - \frac{z}{2}$ and the stoichiometric air-fuel ratio can be expressed as

$$AFR_{\text{stoichiometric}} = \frac{a \cdot \left(M\left(O_2\right) + 3.76 \cdot M\left(N_2\right)\right)}{M\left(C_xH_yO_z\right)} \tag{16}$$

The air mass flow is defined as: $\dot{m}_{\text{air}} = AFR \cdot \dot{m}_{\text{fuel}}$ and lambda was calculated as follows:

$$\lambda = \frac{AFR}{AFR_{stoichiometric}} \tag{17}$$

The air-fuel ratio (AFR) can be determined using either the Brettschneider equation (equation 18) [104] or the modified Spindt equation (equation 19 - 21) [105]. In the former approach, equation 17 is rearranged to obtain the AFR as the product of lambda (computed using the Brettschneider equation) and the stoichiometric AFR.

$$\lambda = \frac{[\mathrm{CO_2}] + \left[\frac{CO}{2}\right] + [O_2] + \left[\frac{NO}{2}\right] + \left(\left(\frac{H/C}{4} \cdot \frac{3.5}{3.5 + \frac{[\mathrm{CO}]}{[\mathrm{CO_2}]}}\right) - \frac{O/C}{2}\right) \cdot ([\mathrm{CO_2}] + [\mathrm{CO}])}{\left(1 + \frac{H/C}{4} - \frac{O/C}{2}\right) \cdot ([\mathrm{CO_2}] + [\mathrm{CO}] + (n \cdot [\mathrm{HC}]))} \tag{18}$$

Here, *[X]* is the gas concentration in volume percent, *H/C* the ratio of hydrogen to carbon in the fuel and *O/C* is the ratio of oxygen to carbon in the fuel, and n is the number of carbon atoms in the hydrocarbon molecule being measured. Alternatively, the AFR can be calculated using the Spindt equation with a modification to account for fuel oxygenation:

$$AFR_{\text{Spindt}} = F_b \cdot \left[11.492 \cdot F_c \cdot \left(\frac{1 + \frac{R}{2} + Q}{1 + R} \right) + \left(\frac{120 \cdot F_h}{3.5 + R} \right) \right] - 4.313 \cdot F_o \quad (19)$$

The variables in this equation are the following ratios:

$$F_b = \frac{P_{CO} + P_{CO_2}}{P_{CO} + P_{CO_2} + P_{CH}}, \quad R = \frac{P_{CO}}{P_{CO_2}}, \quad Q = \frac{P_{O_2}}{P_{CO_2}} \quad (20)$$

and

$$F_c = \frac{12.01x}{12.01x+2.02y+32.0z}, F_h = \frac{2.016y}{12.01x+2.02y+32.0z}, F_o = \frac{32.0z}{12.01x+2.02y+32.0z} \quad (21)$$

3.6. High-pressure/high-temperature chamber

Experiments were performed in an optically accessible high-pressure/high-temperature chamber with a constant volume of 2 L. A 4-stage compressor continuously delivered compressed air at pressures of up to 10 MPa. Electric heaters were used to heat the air (to up to 900 K) before it entered the chamber. The inlet air flow velocity was $\sim$0.1 m/s. Fuel was injected at the bottom of the chamber using a Scania XPI injector with an axially symmetric single-orifice nozzle, 190 μm in diameter. The fuel was supplied via a common rail system connected to a Scania XPI high pressure pump. A more detailed description of the chamber and cameras is presented in earlier publications [106, 107]. Combusting and non-combusting cases were studied at injection pressures of 180 MPa and 120 MPa, respectively, with a gas density of 26 kg/m^3. For non-combusting conditions, the temperature in the spray chamber was set to 623 K (350°C) and the ambient pressure to 4.59 MPa. For combusting conditions, the temperature was set to 823 K (550°C) and pressure to 6.04 MPa. These settings approximate those generated in a heavy duty CI engine operating under low load. At least 30 injection events were studied for each set of experimental conditions, and the subsequent data analysis was based on results averaged over these events. Table 3.7 summarizes the experimental conditions used in this campaign.

Table 3.7.: Experimental conditions used in the high-pressure/high-temperature chamber

		Non-combusting	Combusting
Injection pressure	MPa	120, 180	
Ambient temperature	$^{\circ}C$ (K)	350 (623)	550 (823)
Ambient pressure	MPa	4.59	6.04
Ambient density	Kg/m^3	26	
Injection pulse duration	ms	1.7	3
Frequency of injections	Hz	0.1	
Number of injections	-	30	

3.6.1. Optical setup

Various spray characteristics were measured using several optical methods. The liquid and vapor phase penetration of non-combusting sprays was determined by shadowgraph imaging. As shown in Figure 3.4, a diffuse screen was placed in front of halogen lamps to provide diffuse background illumination. A phantom V1212 high speed video CMOS camera then captured the liquid and vapor penetration images.

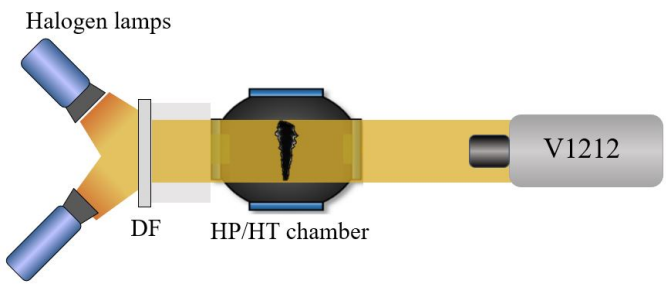

Figure 3.4.: Schematic depiction of the of optical setup for liquid and vapor phase imaging. The diffusor plate (DF) is an iced plate for liquid phase penetration detection and a striped plate for vapor phase detection.

The diffusor plate was an iced plate when measuring liquid penetration, but was replaced with a striped plate when measuring vapor phase penetration. The method of exploiting the recurring contrast between light and dark stripes to visualizes vapor pene-

tration is known as the background grid distortion method. Schardin [108] introduced this method as 'schlieren method no. 2' and it was later adapted for vapor phase imaging by Ochoterena [109]. The optical setup for capturing light extinction, flame luminosity and OH*chemiluminescence is shown in Figure 3.5

Liquid penetration and soot concentrations under combusting conditions were determined by time-resolved two-dimensional light extinction imaging using a laser sheet to enable direct quantitative measurements. The light source was a continuous Nd:YAG laser with a wavelength of 532 nm and a power of 1.5 W. A Phantom V1212 high speed video CMOS camera was used to capture the light extinction by monitoring the diffused laser light passing through the flame. OH*chemiluminescence was recorded with a V7 high speed camera and flame luminescence with an M310 high speed camera. All cameras were synchronized with a frame rate of 27,777 /s using a Stanford Research system signal generator. Several lenses and filters were used to illuminate the area of interest and thus enable recording. The setup is described in detail in Paper II and an earlier publication [106].

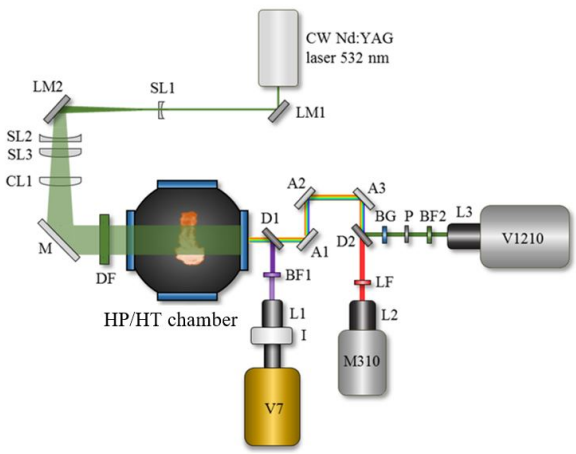

Figure 3.5.: Schematic depiction of the optical set-up used under combusting conditions [107]

3.6.2. Image analysis

Liquid phase penetration length and cone angle

To measure the liquid penetration length, images were cropped and a threshold based on the light intensity profile was identified to define the liquid phase boundary. Figure 3.6 shows a typical raw image while Figure 3.6 shows the same image normalized against the background. The red line indicates the liquid phase boundary and the maximum distance to the nozzle is the penetration length. The spray cone angle α was calculated based on the method introduced by Naber and Siebers [110] with the following equation:

$$\frac{\alpha}{2} = tan^{-1} \cdot \frac{A_{P,\frac{L}{2}}}{(\frac{L}{2})^2} \tag{22}$$

Here, $A_{(p,L/2)}$ is the spray area of the upstream half of the spray and L is the liquid spray penetration length. All reported penetration lengths and cone angles are averages representing at least 30 injection events.

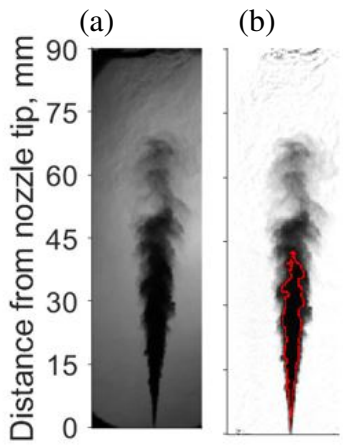

Figure 3.6.: Image processing steps used to determine the liquid penetration length and cone angle. The spray shown was generated using EHD20 at 1.5 ms ASOI with an injection pressure of pinj= 120 MPa.

Vapor phase penetration length

The process used to determine vapor penetration is illustrated in Figure 3.7. The striped background makes it easier to relate images at different stages of processing to one-another. As in the liquid phase analyses, the background was subtracted in the first step.

A threshold was then defined to convert the greyscale image into a binary one. Finally, the vapor penetration length was calculated from the difference between consecutive images.

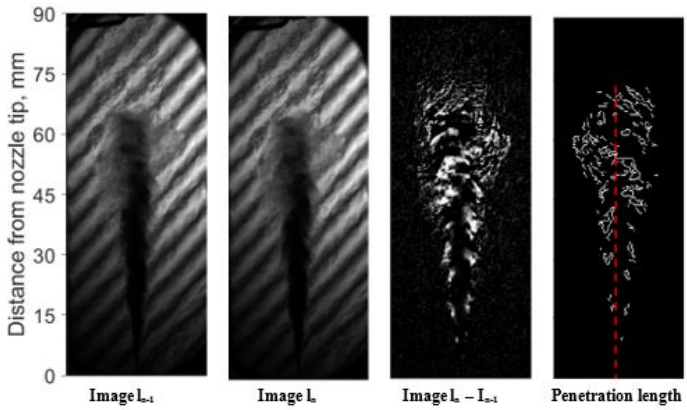

Figure 3.7.: Image processing of measuring vapor phase penetration length. The spray shown was generated using EHD20 at 1.5 ms ASOI with an injection pressure of pinj= 120 MPa.

Laser extinction measurement

The evaluation of laser extinction images is described in detail in an earlier publication [106] and summarized in Paper II. Some important issues relating to the choice of threshold when processing OH*chemiluminescence images and the calculation of the ignition delay are discussed below:

Lift-off length

The lift-off length is commonly defined as distance between the nozzle tip and the mean flame location, which was determined by analyzing OH*chemiluminescence images. Figure 3.8a shows the intensity profile along the fuel jet center line. The threshold used to delineate the boundary of the flame, as shown in Figure 3.8b, was set to a value corresponding to around 50% of the intensity at the 'knee' of the intensity profile. This method is an adaptation of that proposed by Siebers and Higgins [42].

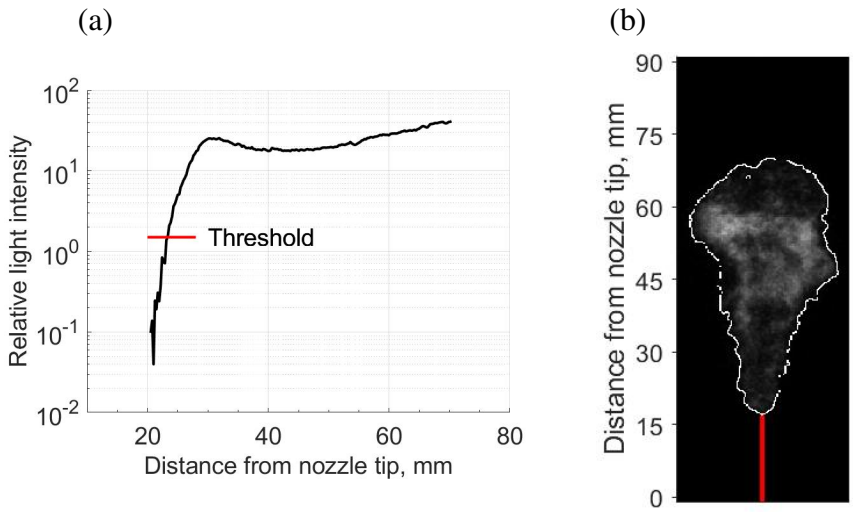

Figure 3.8.: Method to measure lift-off length from OH* chemiluminescence taking Diesel spray at 550°C, 4.6 MPa, p_{inj} = 120 MPa, 3.6 ms ASOI as example.

Ignition delay

The ignition delay is the time between the start of fuel injection and the start of detectable combustion. During this time, the initial fuel air mixture is formed. Physical processes governing the length of the ignition delay include fuel-air mixing, spray breakup and droplet formation, vaporization of the heated fuel and the formation of a combustible vapor air mixture. OH*chemiluminescence imagining can be used to visualize the formation of OH*radicals during high temperature reactions, which begin at the moment of ignition (it should be noted that ignition may occur in several places simultaneously). The ignition delay is thus equal to the length of time between the fuel entering the chamber and the first appearance of OH*chemiluminescence. Longer ignition delays enable the formation of more homogeneous fuel-air mixtures.

The first appearance of soot was detected by analysing flame luminosity images. Therefore, the delay between the start of injection and the first appearance of soot could be determined using an approach analogous to that applied for the ignition delay.

4. Results

This chapter summarizes the experimental results obtained with the tested blends and compares them to those achieved with fossil Diesel and HVO. Findings are presented separately for blends based on long-chain alcohols and those based on OME_{3-5}. The potential of long-chain alcohols was evaluated in heavy duty single cylinder engine tests (Paper I), in a multicylinder heavy duty engine, in light duty single cylinder engine tests, and in spray experiments (Paper II). The effect of changing injection settings and EGR in the single cylinder light duty engine were presented (Paper III). Moreover the performance and emissions of blends containing OME_{3-5} were evaluated in a heavy and light duty single cylinder engine (Paper IV). Further details are provided in the cited and attached publications.

4.1. Evaluation of long-chain alcohols blends

4.1.1. Heavy duty single cylinder engine (Summary of Paper I)

Combustion characteristics

The performance and emissions of a heavy duty CI engine were investigated when using various long-chain alcohol blends and conventional fossil Diesel fuel. The fuel mass flow was kept constant, but because the lower heating values of the blends were lower than that of Diesel (see Table 3.1), the *imep* when using the blends was slightly lower than that for Diesel. Depending on the blend and load case, the reduction in *imep* was between 3.5 % and 6 %. As a result, the blends yielded higher specific fuel consumption than Diesel.

The engine's performance was characterized in terms of its indicated thermal efficiency, the COV in *imep*, and the rate of heat release. The COV was below 1.5 % for all fuels at all loads, indicating that stable combustion was achieved in all cases. Additionally, all fuels yielded similar thermal efficiencies at the A25, B75, and C75 load points. However, at the reference B50 load point, the blends' thermal efficiencies exceeded that of

Diesel. Figure 4.1 shows the MFB50 (i.e., the crank angle where 50 % of the fuel mass is burned) and the combustion duration (MFB90 – MFB10) for all load cases. The first black marker in each line represents Diesel fuel and the coloured markers are the long-chain alcohol blends. MFB50 was slightly advanced for the blends, and their combustion durations were shorter than those of Diesel. Increasing the content of alcohol in the blend increased the rate of combustion, which helped to reduce heating losses and engine out exhaust temperatures; the exhaust gas temperature when using the blends was on average 24 K lower than when using Diesel.

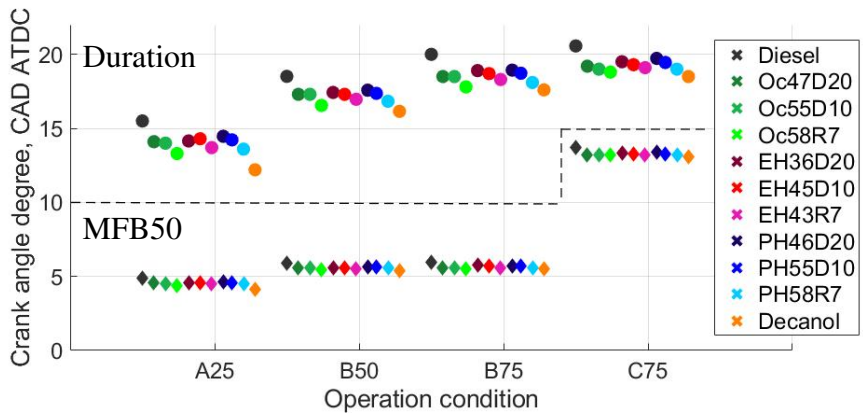

Figure 4.1.: Mass fraction burned 50 % (⧫) and combustion duration (●) in heavy duty engine tests using fossil Diesel and the long-chain alcohol blends for the A25, B50, B75, and C75 load points.

Emissions

HC emissions generated when using the blends were similar to those observed when using Diesel, but the CO emissions when using the blends were significantly lower. Reducing the content of fossil Diesel in the blends from 20 % to 10 % did not cause a linear reduction in emissions. The differences between the emissions of the different blends were within the standard deviation of the measurements. As expected, replacing fossil Diesel with the blends slightly increased NO_x emissions while greatly reducing soot emissions. The reduction in soot emissions became more pronounced as the load increased. The use of blends reduced the soot mass by up to 62 % at the high load point (C75). These results agree with the findings of previous studies on long-chain alcohols, which concluded that these fuels significantly reduce soot emissions relative to fossil

Diesel because of their higher heats of evaporation and because their oxygen content accelerates soot oxidation [25, 111]. Blends containing RME rather than fossil Diesel yielded the lowest particle mass emissions because they contain no aromatic compounds, which are key precursors for soot formation. On average, the use of RME in place of Diesel reduced soot mass by 47 %. However, the blended fuels produced significantly greater numbers of particles with diameters below 23 nm (which is today's cut-off size for particle number measurements). The particle size distribution for the blends was dominated by nucleation mode particles, which could pose a challenge for aftertreatment systems because their filtering efficiency decreases with particle size. The nature and origin of these small particles is currently unknown. Other studies have suggested that smaller particles may originate mainly from lubricating oil [112]. However, this hypothesis cannot explain the increase in small particle emissions observed when using fuel blends with higher oxygen contents in this work. As stated previously, agglomeration mode particles typically account for at least 90 % of the total mass of emitted particulate matter [56]. Because of the agglomerative tendency of particles generated by Diesel combustion, the total mass of emitted particles was higher for Diesel than for the blends, but the opposite was true for particle number emissions.

4.1.2. Multicylinder heavy duty engine: Performance and emissions

Due to confidentiality requirements, results concerning the performance and emissions achieved using the renewable fuel blend EHR7 are mainly presented in relation to those achieved with the fossil Diesel-based fuel B7. Figure 4.2 shows the indicated specific fuel consumption and indicated efficiency for EHR7 relative to those for B7 at all load points from the ESC (except the idle point). The indicated specific fuel consumption for EHR7 was 3.05 % higher than for B7, reflecting the difference in their lower heating values. However, the average thermal efficiency achieved with the blend was 0.6 % higher than for Diesel. The efficiency achieved with the blend in lower load cases (load points 5-7) was lower than in the higher load cases.

Figure 4.3 shows the engine out and system out NO_x emissions for EHR7 relative to B7. Average engine out NO_x emissions were 2.8 % higher for EHR7 than for B7. This was expected based on earlier experiments with the single cylinder engine. However, average system out NO_x emissions for EHR7 were 62.5 % higher than for B7. A strong

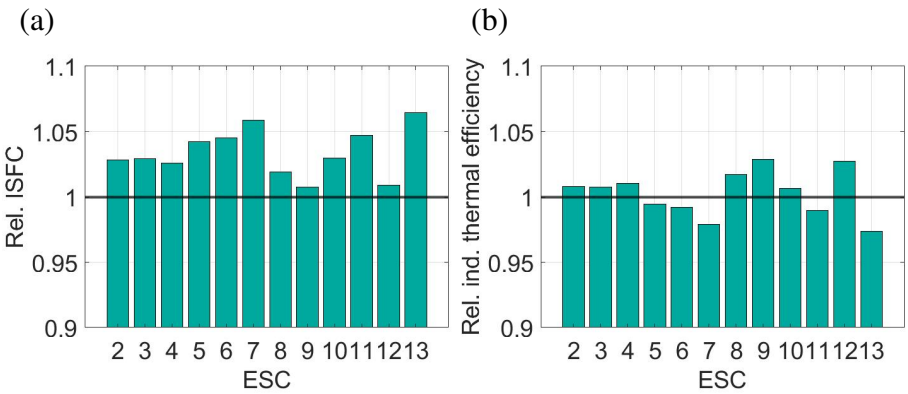

Figure 4.2.: (a) Indicated specific fuel consumption and (b) indicated thermal efficiency for blend EHR7 relative to B7

increase in system out NO_x emissions was observed in the high load cases (8 and 10) and the medium load cases (6 and 12).Owing to very low system-out NO_x levels, the relative differences are higher. But even with higher system out NO_x emissions, the blend EHR7 can meet emission regulations (below 0.4 g/kWh , see Table 1.1) [113].

Figure 4.4 shows the specific soot emissions for EHR7 relative to B7. The use of EHR7 reduced specific soot emissions by up to 72.4 %, and the soot reduction potential was lower in lower load cases (5,7,9, and 11) than in higher load cases. The exhaust temper-

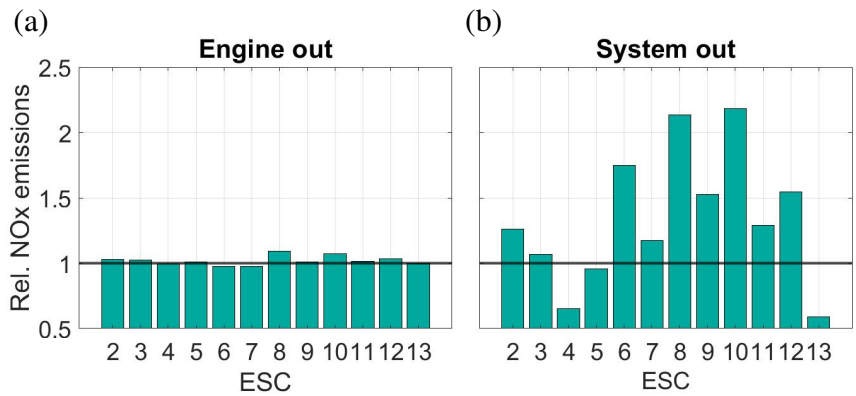

Figure 4.3.: (a) Engine out and (b) system out NO_x emissions for EHR7 relative to B7.

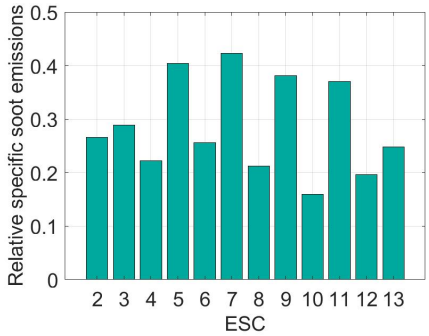

Figure 4.4.: Specific soot emissions for EHR7 relative to B7.

atures for EHR7 were 2.6 % lower than for B7, corresponding to absolute temperature differences of 3.5 to 10.1 K in the low and medium load cases. However, in the high load cases (8 and 10) the reductions in exhaust temperature were 35 K and 37.5 K, which may partly explain the high tailpipe NO_x emissions observed with EHR7.

4.1.3. Light duty engine: Performance and emissions

The results obtained using the blends containing 10 % Diesel in the heavy duty tests were very similar to those obtained using the corresponding 20 % Diesel blends. Therefore, subsequent experiments were performed using only the 20 % Diesel blends and the blends without fossil Diesel and 7 % RME instead.

Combustion characteristics

Additional engine experiments were performed with a light duty engine using a multiple injection strategy. In this case, the engine's performance was investigated using all the long-chain alcohol blends as well as HVO and Diesel as reference fuels. Unlike in the heavy duty engine experiments, the fuel mass flow was adjusted for each blend to compensate for their low lower heating values. Consequently, the specific fuel consumption for the blends was higher than for Diesel, as shown in Figure 4.5. The indicated thermal efficiency was higher for the blends than for Diesel but often lower than for neat HVO. Figure 4.5 also shows the combustion duration and MFB50 for each blend and the reference fuels. When using the blends, MFB50 occurred slightly earlier or at around the same as for Diesel, but the combustion duration was shorter. This is consistent with the

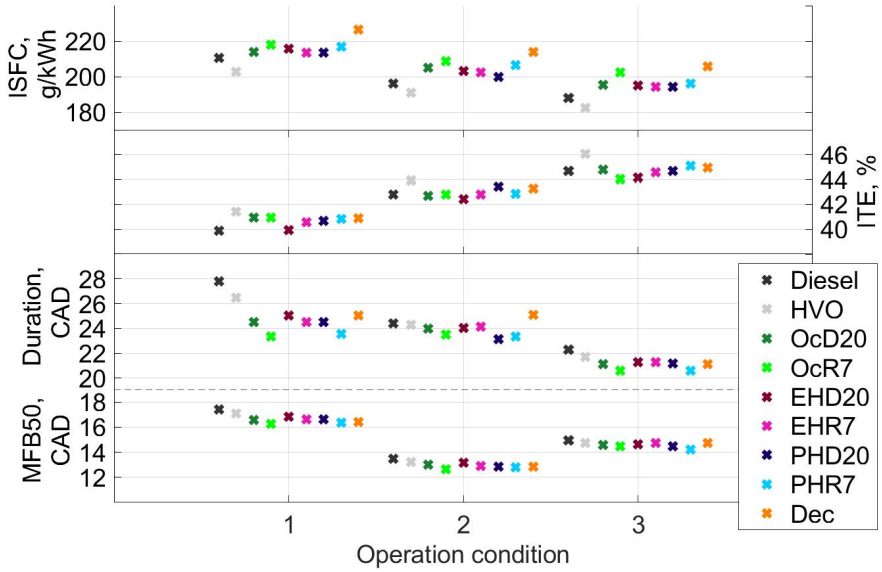

Figure 4.5.: Engine performance of long-chain alcohol blends compared to Diesel (black marker) and HVO (grey marker)

expected increase in the rate of combustion as the alcohol content of the fuel increases. The cylinder pressures and rate of heat release traces for each blend and load case are presented in Figure 4.6. Both the cylinder pressure and the rate of heat release were similar for all tested fuels. For the blends, the peak heat release occurred slightly later in load case 2 (1810 rpm, 0.74 MPa *imep*) than in other load cases.

Emissions

Indicated specific NO_x and soot emissions for the blends and reference fuels are shown in Figure 4.7. The blends' NO_x emissions were higher than those for Diesel and HVO. Notably, in the medium load cases 1 (0.88 MPa *imep*) and 3 (1.12 MPa *imep*), the blends' NO_x emissions were substantially higher than for Diesel and HVO; for the blend PHR7, they were three times those for Diesel. However, the blends' soot emissions were much lower than those for Diesel. While all blends had comparatively low soot emissions, those containing RME instead of Diesel emitted the least soot (Figure 4.7a). The reduction in soot emissions was thus accompanied by increased NO_x emissions, in keeping

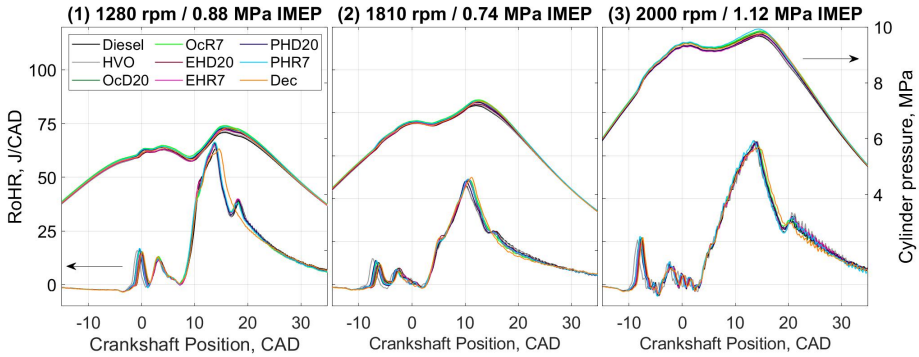

Figure 4.6.: Rate of heat release and pressure traces for light duty engine tests

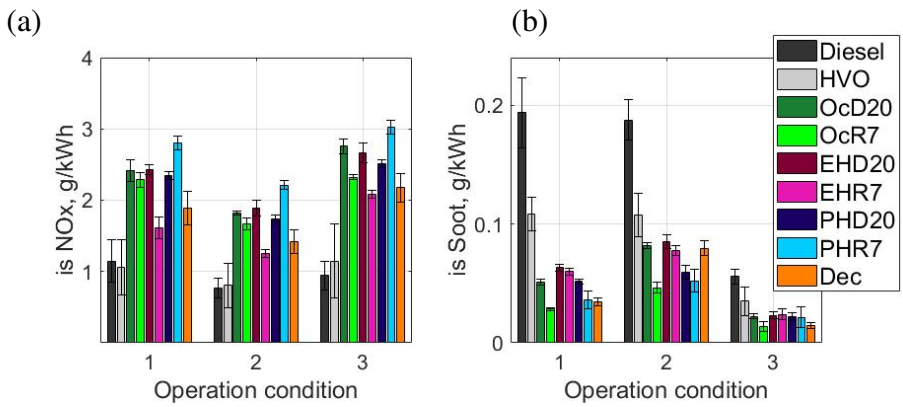

Figure 4.7.: (a) Indicated specific NO_x and (b) indicated specific soot emissions

with the typical trade-off observed for CI engines.

The particle size distributions for the blends and reference fuels are shown in Figure 4.8. In all cases, the agglomeration mode predominated. For load cases 1 and 2, the distributions for all fuels feature a shoulder in the diameter range between 20 nm and 60 nm. Particle number emissions for the blends were lower than for Diesel when considering particles with diameters above 60 nm. A similar result was observed for load case 3. However, particle number emissions in this high load case were lower than in the lower load cases. In all load cases, the peak of the PSD occurred at a lower geometric mean diameter for the blends than for Diesel. The PSD differed from the one obtained from

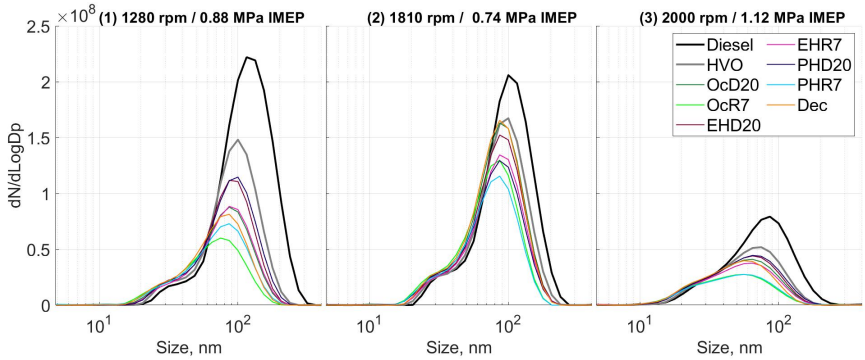

Figure 4.8.: Particle Size distribution for all three load cases.

the combustion in the heavy duty single cylinder engine. A bimodal PSD was obtained with a single injection strategy in HD experiments. With a multi injection strategy, particle agglomeration was facilitated. Details on the influence of the injection stategy can be found in Section 4.1.4.

Soot morphology

Soot samples were taken from fossil Diesel and the fuel blend EHR7 for operation condition 1 (1280 rpm, 0.88 MPa *imep*, see Table 3.6). A transmission electron microscope (TEM) and image software was used to analyze soot morphology characterized by primary particle diameter, fringe length, fringe separation and tortuosity [114].
Figure 4.9 shows TEM images from Diesel and EHR7 at different magnifications. Stacked graphene layers, which form the soot particle, are called fringes. Fringe length, separation length and tortuosity were similar for both fuels at the selected operating condition. The primary particle size was smaller, corresponding to increased soot oxidation and thus lower particle mass emissions.

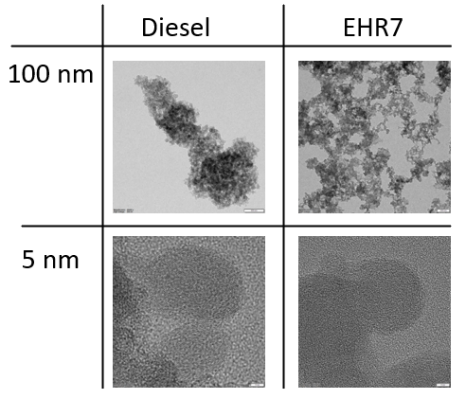

Figure 4.9.: TEM images from fossil Diesel fuel and EHR7 blend

4.1.4. Light duty engine: Influence of EGR and injection strategy on particle emissions (Summary of Paper III)

As shown in the heavy duty (single injection) and light duty (multiple injection) tests, the injection strategy influenced the PSD. To better understand the changes in PSD, the injection strategy and EGR were varied in a single cylinder light duty engine using HVO, fossil Diesel, and a blend containing 37 % EH, 56 % HVO and 7 % RME by volume. The effects of different injection strategies (main, main/post, double pre/main, double pre/main/post injection) and EGR levels (0 % and 19 %) on the PSD and emissions of NO_x and soot were investigated while keeping the crank angle for MFB50, fuel consumption, and *imep* constant. The results obtained are presented in Paper III and summarized below.
The indicated thermal efficiencies were similar for all tested fuels and injection strategies. Heat release analysis revealed a significant effect of the cetane number when using main and main/pre injection strategies both with and without EGR. HVO has a higher CN than Diesel and the blend, so the ignition delay was shorter for HVO. When using a double pre-injection, the ignition delay (i.e., the period between the start of injection and MFB10) shortened equally for all tested fuels, independently of the use of EGR.

With a double pre-injection and 19 % EGR, the mass fraction of the fuel burned in premixed combustion mode was reduced, leading to a greater soot mass and a PSD dominated by agglomeration mode particles (diameters > 23 nm). However, NO_x emis-

sions did not differ appreciably. The number of particles increased when using a double pre-injection. Without EGR, soot emissions decreased while NO_x emissions increased due to the higher in-cylinder temperature. The particle size distribution was dominated by small nucleation mode particles. In contrast to the 19 % EGR scenario, particle number emissions fell when using a double pre-injection without EGR. Many publications suggest that a post injection can reduce engine out emissions by enhancing mixing and/or raising the in-cylinder temperature due to additional heat release [62]. The actual reduction in emissions achieved using post-injection strategies seems to depend on the duration of each injection and the dwell times between the injections, as well as the engine operating conditions. In the studied light duty engine, the post injection slightly reduced soot emissions in the 19 % EGR case but not in cases without EGR. The double pre-injection was thus identified as the strategy with the greatest influence on combustion and emissions, irrespective of the EGR rate.

With a double pre-injection with or without EGR, the soot mass reduction achieved by using the blend instead of Diesel was greater than when not using the double pre-injection. The highest soot mass reduction was achieved with 19 % EGR and a double pre/main/post injection. However, the double pre-injection reduced the time available for pre-mixing, so total soot mass emissions were higher than when using the main or main/post injection strategies. With EGR and a double pre-injection, the PSD was dominated by agglomeration mode particles for all fuels. Without EGR, the PSD was dominated by nucleation mode particles and the particle mass was about ten times lower than in the 19 % EGR case. In contrast, when EGR was used, particle number emissions were lower for all fuels with a double-pre injection than with any alternative injection strategy.

PSD measurements were performed with and without removing volatile organics using a thermodenuder. Figure 4.10 shows typical measurements obtained with and without the thermodenuder and the corresponding capture efficiency for the double pre/main/post injection strategy with 19 % and 0 % EGR. The capture efficiency is the difference in the number of particles detected before and after removing volatile organics with the thermodenuder, divided by the number detected before removal (see equation 3). The PSD was dominated by the agglomeration mode in the 19 % EGR case and by the nucleation mode without EGR. When using EGR, average capture efficiency was

lower for the EHR7 blend than for the other fuels, but the standard deviations indicated that the difference was not significant. Without EGR, the blend had the highest capture efficiency for most particle sizes and Diesel had the lowest.

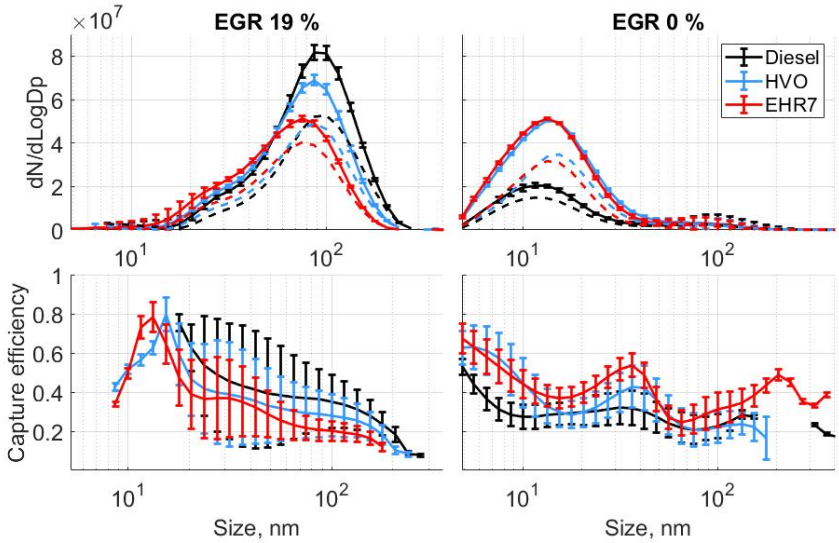

Figure 4.10.: PSD and capture efficiency for the double pre/main/post injection strategy with 19 % EGR (left) and 0 % EGR (right). In the upper images, continuous lines indicate results obtained without the thermodenuder while dashed lines represent those obtained with the thermodenuder. Standard deviations are not shown for the PSD after passage through the thermodenuder for clarity. However, the errors were approximately equal for both measurements.

4.1.5. High pressure/high temperature constant volume chamber (Summary of Paper II)

Paper II focuses on the spray characteristics of fuel blends based on the long-chain alcohol 2-ethylhexanol, HVO, and fossil Diesel or RME, and compares them to sprays of neat Diesel and HVO. Experiments were performed in an optically accessible high-pressure/high temperature chamber under non-combusting (623 K, 4.59 MPa) and combusting conditions (823 K, 6.04 MPa). Injection pressures of 120 MPa and 180 MPa were used at a stable ambient gas density of 26 kg/m3. Several optical imaging techniques were used to obtain information about the spray characteristics. The liquid and vapor penetration length were captured by means of shadow imaging under non-combusting conditions. Under combusting conditions, time-resolved two-dimensional light extinction imaging was performed. The use of monochromatic laser light made it possible to acquire direct quantitative measurements even in strongly luminescent flames. Flame luminosity and OH* chemiluminescence images were acquired simultaneously.

The liquid penetration lengths for the blends and HVO were found to be higher than that for Diesel under non-combusting conditions, but all of the tested fuels had similar vapor penetration lengths. The higher liquid penetration lengths of the blends may be due to the higher latent heat of evaporation of 2-ethylhexanol, which means that more energy is required to induce a transition from the liquid to the vapor phase.

The fuels' ignition delay times were compared under combusting conditions. Despite having similar CN values to Diesel, the alcohols had longer ignition delays. Moreover, HVO and Diesel had similar ignition delays even though the CN of HVO is appreciably higher than that of Diesel. CN measurements were done in a Cooperative Fuel Research (CFR) engine under standard physical conditions (ISO 5165)[96]. The observed ignition behaviour of the blends differed from that which would be expected given their calculated CN values, possibly because conditions in the spray chamber experiments differ from those in the CFR engine. Another possible reason is that the method for measuring the CN was designed for petroleum-derived fuels; while it can be applied to oxygenated fuels, the relationship between the CN and performance in standard engines is not fully understood in such cases. The operating conditions in the CFR engine are defined by the volumetric fuel flow and start of ignition. Consequently, the fuel energy introduced

varies and is usually lower with oxygenated fuels. As a result, the operating points vary, which can introduce uncertainty into the measurements.

Image processing of flame luminosity data revealed the time after the start of injection at which soot became visible. In accordance with the longer ignition delay of the alcohol blends, soot formation with the blends began later than with HVO and Diesel. The lift-off length (i.e. the distance between the nozzle and the location of autoignition) was determined based on the detection of OH* radicals, and was similar for HVO and Diesel. The similarity of the spray characteristics of Diesel and HVO is consistent with previous literature reports. The blends' lift-off lengths were longer than that of Diesel. Longer lift-off lengths and ignition delays provide more time for air-fuel mixing before ignition, resulting in more homogeneous combustion. The longer ignition delays and lift-off lengths observed for the blends can be attributed to the alcohols' higher latent heat of evaporation. Due to the lack of soot precursors in the EHR7 blend and its shorter residence time, soot formation was suppressed. Consequently, this fuel produced the lowest soot volume fraction.

4.2. Evaluation of Poly (oxymethylene) dimethyl ether blends (Summary of Paper IV)

The main findings concerning the potential of OME_{3-5} blends as renewable drop-in fuels are presented in Paper IV and summarized below.

4.2.1. Heavy duty engine

Combustion characteristics

The performance and emissions of a heavy duty CI engine were investigated when keeping *imep* constant. To compensate for the slightly lower heating value of the blends, the injection duration was increased. The indicated thermal efficiency, indicated specific fuel consumption, combustion duration (MFB90-MFB10), and the mass fraction at which 50 % of the fuel is burned (MFB50) for the heavy duty engine tests are plotted in Figure 4.11. The first dark marker for each operating point shows the reference value obtained using Diesel, and the second marker (in grey) shows the result obtained with HVO. Results for blends are plotted in order of increasing oxygen content (6 %, 13 %,

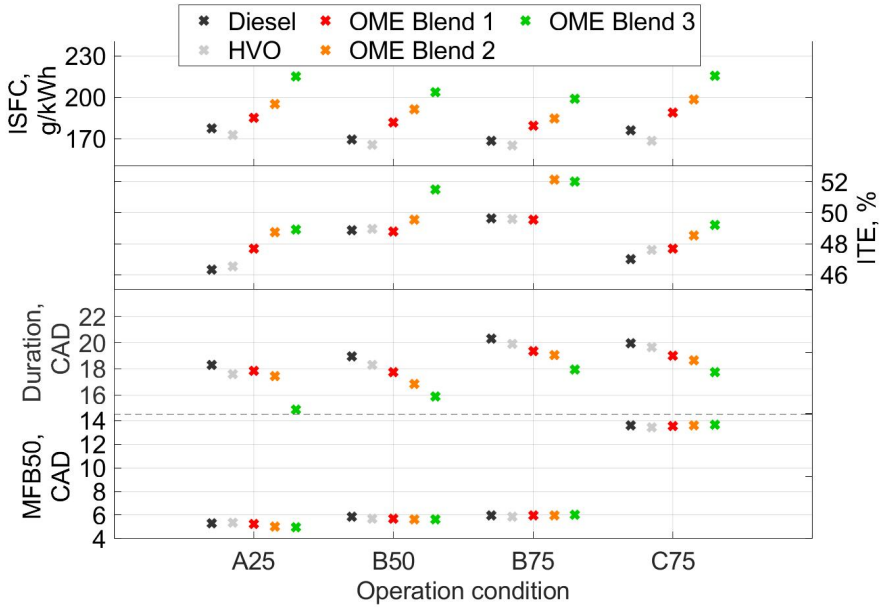

Figure 4.11.: Heavy duty engine: Indicated specific fuel consumption (*isfc*), indicated thermal efficiency (ITE), combustion duration (MFB90-MFB10) and MFB50.

and 18 % by mass). OME Blends 2 and 3 yielded higher efficiencies than Diesel for all load cases, but the efficiency of OME Blend 1 was similar to that for HVO and Diesel in the B50, B75, and C75 load cases. The average *isfc* for HVO was 2.8 % lower than that for Diesel. Conversely, the lower LHV of the blends necessitated the use of longer injection durations, causing *isfc* to increase by 6.4 % on average relative to Diesel. While the crank angle at which 50 % of the fuel is burned was kept constant for all the fuels, the combustion duration was shorter for the blends than for Diesel and HVO. The blends also yielded lower exhaust losses than Diesel due to their faster combustion, which partly explains their superior thermal efficiency.

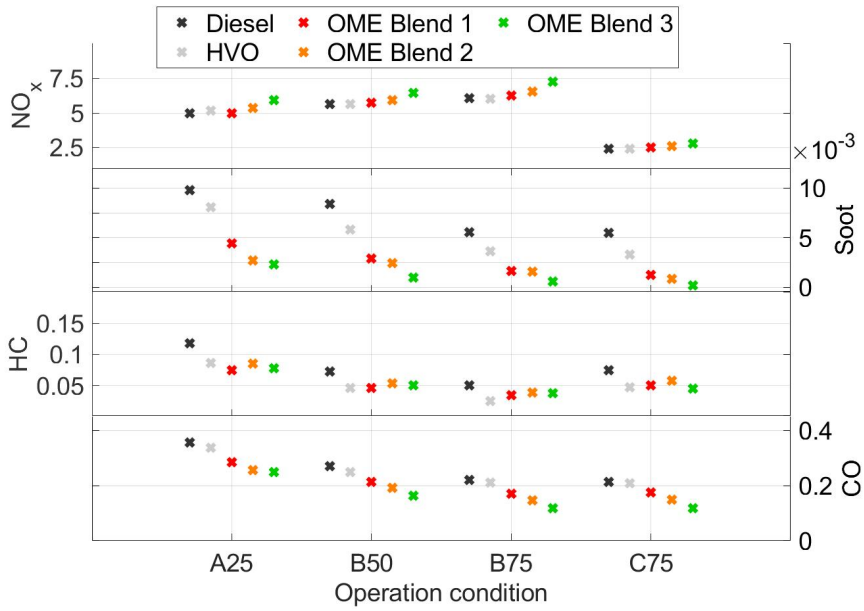

Figure 4.12.: Heavy duty engine: Indicated specific exhaust gas emissions in g/kWh.

Emissions

As shown in Figure 4.12, the NO_x emissions achieved with the OME_{3-5} blends were slightly higher than those for HVO and Diesel, and increased with fuel's oxygen content. However, the soot emissions achieved with the blends were much lower than those for Diesel, meaning that their use alleviated the soot-NO_x trade-off typical for CI combustion. Soot mass emissions decreased as the oxygen content of the fuel increased. This is consistent with previous reports concerning the effect of oxygen on soot emissions [111, 115]. Figure 4.12 also shows that soot emissions were reduced by over 50 % by adding 7 % of OME to the fuel blend (see Table 3.2, OME Blend 1) in all load cases. As shown in Figure 8, the indicated specific HC emissions for HVO and the OME_{3-5} blends were similar and substantially lower than those for Diesel. Additionally, the indicated specific CO emissions decreased as the fuel's content of OME_{3-5} increased.

The PSDs of both Diesel and HVO were dominated by agglomeration mode particles with diameters above 20 nm (depending on the operating point). For the blends, nucleation mode particles dominated and the peak of the PSD was between 7 - 10 nm.

The number of small particles increased with the fuel's content of OME_{3-5} (and thus with its oxygen content). Agglomeration of soot particles is less likely due to the lower number of primary particles (caused by the absence of precurser molecules like PAH). Further experiments are required to determine the composition of the particles emitted in each case, but literature reports suggest that particles originating from lubrication oil may contribute to the observed nucleation mode emissions [112].

4.2.2. Light duty engine

Combustion characteristics

Three blends containing OME_{3-5}, HVO, RME, and EH were tested in a light duty engine under three load conditions. Figure 4.13 summarizes the resulting engine performance and combustion data.

The average *isfc* for HVO was 2.5 % lower than that for Diesel, and the low LHV of

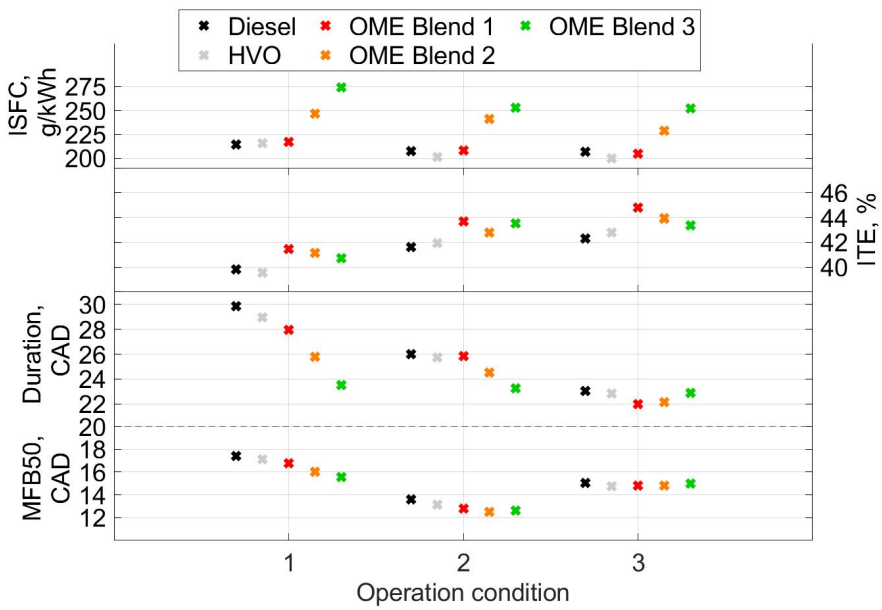

Figure 4.13.: Light duty engine: Indicated specific fuel consumption (*isfc*), indicated thermal efficiency (ITE), combustion duration (MFB90-MFB10) and MFB50.

the blends necessitated the use of longer injections. Consequently, the *isfc* values for OME Blends 1-3 were 2.3 %, 16.7 %, and 24.8 % higher, respectively, than that for Diesel. The blends yielded a higher indicated thermal efficiency than Diesel, which can be attributed to the advancement of MFB50 and the reduced combustion duration. Additionally, the blends reduced heat losses and lowered the exhaust gas temperature by 10 K on average relative to Diesel. The peak pressures were higher for the blends and highest for OME Blend 3.

Emissions

The observed emissions trends resembled those seen in the heavy duty engine tests. For OME Blend 1, the NO_x emissions were similar to those of HVO in the lower load cases (1 and 2) when the standard deviation was taken into account (see Figure 4.14a). For OME Blends 2 and 3, average NO_x emissions were around 33 % higher than for Diesel. Soot emissions for OME Blend 1 were about half of those of Diesel in the medium load case (load 1) and were comparable to those of HVO in higher load cases (see Figure 4.14b). Soot emissions for all fuels decreased with increasing load, in agreement with previous findings [116]. The soot reduction potential decreased with increasing load. When using OME Blend 3, soot emissions were 94 %, 95 %, and 74 % lower than for Diesel in load cases 1-3, respectively,

The blends also reduced particle number emissions relative to Diesel. The PSDs from the light duty engine lacked the bimodal distribution seen in the heavy duty case; there

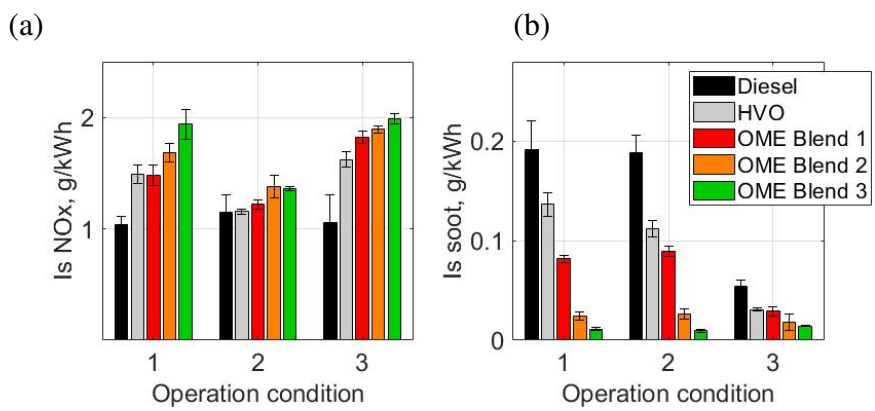

Figure 4.14.: (a) Indicated specific NO_x and (b) indicated specific soot emissions.

was no peak in the nucleation mode range, probably because a multi-injection strategy was used (Paper III, [85]). Instead, particle number emissions decreased as the fuel's content of OME_{3-5} increased. The peak of the particle size distribution curve occurred at a lower geometric mean diameter than for Diesel.

5. Summary and Conclusions

This chapter summarizes the experimental results obtained using the different fuel blends and answers the research questions concerning the drop-in potential of renewable fuel blends based on long-chain alcohols and OME_{3-5} (see Chapter 1.2).

5.1. Summary of experimental work

This work was performed with the aim of identifying viable and sustainable drop-in fuels for compression ignition engines. Blends were used instead of neat components to overcome the undesirable properties of the neat fuel components and obtain blends with properties similar to Diesel, enabling their use as drop-in fuels for existing Diesel engines. The content of fossil Diesel in such blends should be as low as possible; ideally, it would be completely substituted by renewable alternatives.

In the first series of experiments, blends of long-chain alcohols, HVO, and RME or Diesel were investigated in a heavy duty engine, a light duty engine, and a high pressure/high temperature constant volume chamber. Compared to Diesel, the blends had slightly higher specific fuel consumption values in both the light and heavy duty engine experiments due to their smaller lower heating values. However, the thermal efficiencies of the engines when using the blends were similar to or higher than those for Diesel, depending on the load conditions. The long-chain alcohol blends also markedly reduced the combustion duration and emissions of soot and CO relative to Diesel. The soot emission reduction potential increased with the share of alcohol in the blend. However, when a single fuel injection strategy was used together with exhaust gas recirculation (both are standard in heavy duty engines), the use of the blends increased the number of nucleation mode particles emitted. These small particles may be inefficiently removed by current aftertreatment systems. Additionally, new emissions standards are being introduced that will reduce the cut-off diameter for the counting of exhaust soot particles

to 10 nm. Therefore, any increase in small particle emissions resulting from the use of renewable fuels must be considered carefully. The nature and origin of these particles is currently unknown, although it was shown that they consist partly of volatile organic compounds that can be removed by a thermodenuder. It may be that they originate in part from lubrication oil, as suggested in the literature. Or the number of primary particles is too low to engage in agglomeration.

Similar performance trends were observed in tests using the light duty engine. However, the use of long-chain alcohol blends in this case strongly increased NO_x emissions, which may present a barrier to their use as drop-in fuels. The performance and emissions data for the two engines revealed no appreciable differences between the studied alcohol blends and showed that all of them could potentially serve as substitutes for fossil Diesel.

The optical measurements confirmed the results of the engine tests and provided valuable information about the spray characteristics of the blends. In particular, they revealed that both the oxygen content of the fuel and the latent heat of vaporization of its components have significant effects on its spray characteristics and thus the emissions it generates when burned. Additionally, it was found that the CN values determined for the blends did not accurately predict their ignition quality. This was attributed to the difference between the physical conditions in the CFR engine and those of the experiments used to determine the CN, and to uncertainties relating to the suitability of the method of CN determination when applied to oxygenated fuels.

HP/HT chamber experiments could not be performed with neat n-decanol due to its high viscosity. While engine experiments with n-decanol were possible, its potential as a drop-in fuel was therefore judged to be lower than that of the other renewable fuel candidates assessed in this work.

To evaluate the potential of blends containing OME_{3-5} as drop-in fuels, heavy and light duty engine tests were performed. Advantages of OME_{3-5} include its high oxygen content and lack of carbon-carbon bonds, both of which should help reduce soot emissions. Its most notable disadvantage is material incompatibility. To exploit these advantages while mitigating material incompatibility, blends were created containing different pro-

portions of OME_{3-5}, a mixture of vegetable oils (HVO and RME), and the long-chain alcohol 2-ethylhexanol (which was added to ensure miscibility). Three blends were designed with oxygen contents of 6.4 %, 12.8 %, and 17.8 % by mass.
The trends observed with these blends in heavy and light duty engines were similar: Diesel, HVO and OME Blend 1 all yielded similar efficiency values that were lower than those for OME Blends 2 and 3. The blends' fast combustion reduced heat losses in the exhaust relative to those observed with Diesel, but their comparatively small lower heating values caused *isfc* to increase. Soot emissions were reduced by over 50 % upon adding 7 % of OME_{3-5} by volume to the fuel (depending on the load conditions), while NO_x emissions were only slightly increased. The increase in NO_x emissions was less pronounced than for the long-chain alcohol blends tested in the light duty engine, making the soot-NO_x trade-off more favourable for the OME_{3-5} blends. As the content of OME_{3-5} increased, soot emissions fell strongly. In keeping with the results obtained for the long-chain alcohol blends, burning OME_{3-5} blends in the heavy duty engine generated high emissions of small particles; nucleation mode particle number emissions increased with the fuel's content of OME_{3-5}. However, this behaviour was not observed in the light duty engine tests.

In conclusion, blends with low shares of OME_{3-5} significantly reduced soot emissions while maintaining engine performance. However, further research is needed to investigate the compatibility of blends containing different levels of OME with common engine materials in order to properly assess the potential of such blends as drop-in fuels.

5.2. Conclusions

This section answers the research questions concerning the drop-in potential of blends containing long-chain alcohols and OME_{3-5} by assessing the studied blends' effects on engine efficiency, specific fuel consumption, and emissions. Additionally, outstanding challenges relating to renewable fuel blends are discussed.

Potential of long-chain alcohol blends as drop-in fuels
Experimental investigations showed that blends containing long-chain alcohols, HVO, and RME can be used as drop-in fuels in heavy duty and light duty CI engines without harming engine performance: depending on the load conditions, the use of such blends

maintained or increased engine efficiency relative to that achieved with Diesel. However, fuel consumption increased slightly. Differences in engine performance between the blends were within one standard deviation. However, the emissions of gases and soot depended on the fuel's oxygen content. In general, blends with higher oxygen contents and without aromatic constituents (i.e., without added Diesel) yielded greater reductions in soot emissions.
Life cycle analysis indicated that replacing fossil Diesel for CI engines with blends based on the C_8 alcohol 2-ethylhexanol could strongly reduce well-to-wheel global warming potential.

Challenges relating to the use of long-chain alcohol blends as drop-in fuels

There was no evidence of damage to the engine hardware due to the use of blends containing long-chain alcohols, HVO, RME, and a lubricating additive. However, the long-term effects of using such blends in existing engines (particularly on potentially vulnerable components such as filters and rubber parts) are unknown.
The use of the C_{10}-alcojhol n-decanol as a fuel may be complicated by its high viscosity. Additionally, the viscosities of blends containing the isomer 2-propylheptanol were at the upper limit of the range permitted by the EN 590 regulations. Therefore, C_8 alcohols appear better than longer-chain alcohols as drop-in fuel components.
Light duty engine tests revealed that all tested fuel blends strongly increased NO_x emissions; depending on the load conditions, NO_x emissions were increased by factors of two or more compared to Diesel. Increased NO_x emissions were also observed in the heavy duty engine tests, although the increase was less severe than in the light duty case. Additionally, multicylinder engine tests revealed that the alcohol blends increased system out NO_x emissions. This suggests that existing SCR systems perform less well with such blends than with B7 (for which they are calibrated).
Another notable issue was the high emissions of small particles when using a single injection strategy. Single injection strategies are commonly used in heavy duty engines and one was tested in the light duty engine (see Paper III). Particle size measurements in the heavy duty engine experiments revealed increased emissions of small particles with diameters below the current legal cut-off value of 23 nm.

Potential of poly(oxymethylene) dimethyl ether blends as drop-in fuels

For the duration of the experiments, blends containing OME_{3-5}, HVO, RME and EH

could be used as drop-in fuels in heavy and light duty CI engines. They maintained or increased engine efficiency (relative to Diesel), depending on the load case. However, due to their low lower heating values, they slightly increased specific fuel consumption. These trends became stronger as the content of OME_{3-5} in the blend increased.
OME Blend 1, whose content of OME_{3-5} was 7 % by volume, yielded half the indicated specific soot emissions of Diesel in heavy duty engine tests. OME Blend 3, which contained 27 % OME_{3-5}, reduced soot emissions by 97 % in the highest load case. These dramatic soot reductions were attributed to the high oxygen content of OME_{3-5} and its lack of carbon-carbon bonds and aromatic structures. The reductions in soot emissions became more pronounced as the load increased.

Challenges relating to the use of poly(oxymethylene) dimethyl ether blends as drop-in fuels

NO_x emissions increased with the fuel's content of OME_{3-5} and with the engine's load. The average increase in NO_x emissions was 2.9 % for OME Blend 1 and 18.1 % for OME Blend 3 in the heavy duty engine. More pronounced increases were observed in the light duty tests, ranging from 29 % on average for OME Blend 1 to 50 % on average for OME Blend 3.

Additionally, OME_n is known to adversely affect engine hardware. Basic material tests were done to estimate the influence of the ether on rubber parts before using OME_n in the engine, revealing that immersion in pure OME_n caused swelling of rubber and plastic components. Therefore, the blends' content of OME_n was kept below 27 % by volume. Further research is needed to determine how much OME_n can be blended with vegetable oils without harming engine hardware. Engine experiments have been performed using neat OME_n (see for example [94]), but this required the replacement of seals with resistant materials (e.g. Teflon). Neat OME_{3-5} promises soot-free combustion, but our results obtained using blends containing OME_{3-5} (Paper IV) showed that soot emissions can be very strongly reduced even when using blends containing only 27 % OME_{3-5} by volume. This is promising and suggests that it may be possible to identify a blend that strikes a favourable balance between soot reduction and material compatibility.

Another challenge of OME_n is the technological maturity of its production process. Since the relative abundance of oxymethylene chains with different lengths varies from batch to batch, miscibility problems can occur. Further experiments are needed to determine the usefulness of adding an emulsifier to OME blends. Alternatively, the content of OME_{3-5} in the blends could be optimized to ensure miscibility with vegetable oils.

Concluding remarks

The term drop-in fuel means that no changes in engine hardware or software calibration should be required. The engine hardware was not detectably harmed during any of the experiments reported here. However, to ensure the safety of such blends, long-term material tests are needed.

Engine performance was successfully maintained with blends based on long-chain alcohols and OME_{3-5}. But replacing Diesel with such blends slightly increased specific fuel consumption, strongly increased NO_x emissions from the light duty engine, and increased emissions of small particles from the heavy duty engine. These issues could hinder the use of such blends as drop-in fuels. One solution can be lower shares of alcohols in the blend.

6. Outlook and future work

The use of the renewable fuel blends changed the nature of the emitted soot particles. Combustion with EGR while using a single injection strategy increased emissions of smaller particles in both heavy duty and light duty engine tests; additionally, changes in particle morphology and soot reactivity have been reported when using renewable fuels [114, 117]. All these factors could reduce the performance of exhaust aftertreatment systems. Future studies in this area should therefore evaluate the effect of small soot particles on Diesel particulate filters. Additionally, because the cut-off size for counting of particulate emissions is expected to be reduced to 10 nm in the upcoming Euro VII standards [53], both engine out and tail pipe emissions should be measured in these studies. Finally, the influence of elevated engine out NO_x emissions on the ability of selective catalytic reaction (SCR) systems to convert engine out NO_x into nitrogen and water must be investigated; new fuels may require re-tuning of SCR and UDS systems.

Bibliography

[1] International Energy Agency (IEA) , "CO_2 emisions from fuel combustion," *IEA Publications*, 2019.

[2] A. Sydbom, A. Blomberg, S. Parnia, N. Stenfors, T. Sandström, and S. Dahlén, "Health effects of diesel exhaust emissions," *European Respiratory Journal*, vol. 17, pp. 733–46, 2001.

[3] European Environment Agency (EEA), "Greenhouse gas emissions from transport in the EU, by transport mode and scenario," 2020.

[4] European Automobile Manufacturers Association, "New Passenger Car Registrations By Alternative Fuel Type in the European Union," no. forth quarter, 2020.

[5] "Fordonsbestånd och mobilitet," Trafikanalys/SCB, Tech. Rep., 2021.

[6] Kraftfahrt-Bundesamt, "Durchschnittliches Alter von PkW in Deutschland in den Jahren 1960 bis 2020," 2021.

[7] DieselNet, "Emission standards - Summary of worldwide engine and vehicle emission standards," 2021. [Online]. Available: https://www.dieselnet.com/standards/

[8] M. Lapuerta, M. Villajos, J. R. Agudelo, and A. L. Boehman, "Key properties and blending strategies of hydrotreated vegetable oil as biofuel for diesel engines," *Fuel Processing Technology*, vol. 92, pp. 2406–2411, 2011.

[9] T. Hartikka, M. Kuronen, and U. Kiiski, "Technical Performance of HVO (Hydrotreated Vegetable Oil) in Diesel Engines," *SAE Technical Paper 2010-01-1585*, 2012.

[10] P. C. Shukla, S. Shamun, L. Gren, V. Malmborg, J. Pagels, and M. Tuner, "Investigation of Particle Number Emission Characteristics in a Heavy-Duty Compression Ignition Engine Fueled with Hydrotreated Vegetable Oil (HVO)," *SAE Int. J. Fuels Lubr. 2018-01-0909*, vol. 11, pp. 495–505, 2018.

[11] Ö. Andersson and P. Börjesson, "The greenhouse gas emissions of an electrified vehicle combined with renewable fuels: Life cycle assessment and policy implications," *Applied Energy*, vol. 289, p. 116621, 2021.

[12] H. S. Hess, J. Szybist, A. L. Boehman, P. J. A. Tijm, and F. J. Waller, "Impact Of Oxygenated Fuel On Diesel Engine Performance And Emissions," in *Proceedings of NHTC'01, 35th National Heat Transfer Conference*, vol. NHTC01-114, 2001.

[13] J. Manin, S. Skeen, L. Pickett, E. Kurtz, and J. E. Anderson, "Effects of Oxygenated Fuels on Combustion and Soot Formation/Oxidation Processes," *SAE Int. J. Fuels Lubr. 2014-01-2657*, vol. 7, pp. 704–717, 2014.

[14] J. Campos-Fernández, J. M. Arnal, J. Gómez, and M. P. Dorado, "A comparison of performance of higher alcohols/diesel fuel blends in a diesel engine," *Applied Energy*, vol. 95, pp. 267–275, 2012.

[15] B. Heuser, F. Kremer, S. Pischinger, J. Julis, and W. Leitner, "Optimization of diesel combustion and emissions with newly derived biogenic alcohols," *SAE Technical Paper 2013-01-2690*, 2013.

[16] European Committee for Standardization, "EN 590: Automotive fuels - Diesel - Requirements and test methods, European Committee for Standardization," 2009, ref. No. EN 590:2009.

[17] Neste, "Safety Data Sheet: Neste Diesel fuel, sulphur free," 2017.

[18] Sigma-Aldrich, "1-Octanol, 95446," *Safety Data Sheet*, 2015.

[19] Sigma-Aldrich, "1-Decanol, W236500," *Safety Data Sheet*, 2015.

[20] Perstorp BioProducts AB, "2-Ethylhexanol," *Safety Data Sheet*, 2016.

[21] Perstorp BioProducts AB, "2-Propylheptanol," *Safety Data Sheet according to 1907/2006/EC, Article 31*, pp. 1–12, 2015.

[22] Neste Oil, "Hydrotreated vegetable oil (HVO)-premium renewable biofuel for diesel engines," *Safety Data Sheet*, 2014.

[23] Perstorp BioProducts AB, "RME - Perstorp BXN," *Safety Data Sheet according to 1907/2006/EC, Article 31*, 2016.

[24] J. Borovský, "Report OME-Mix 3-5," ASG: Analytik-Service Gesellschaft, Tech. Rep., 2018.

[25] D. R. Tree and K. I. Svensson, "Soot processes in compression ignition engines," *Progress in Energy and Combustion Science*, vol. 33, pp. 272–309, 2007.

[26] Swedish Energy Agency, "Energy in Sweden 2020 - An Overview," pp. 1–14, 2020.

[27] International Energy Agency (IEA), "Renewables 2020, Analysis and forecast to 2025," Tech. Rep., 2020.

[28] R. Arvidsson, S. Persson, M. Fröling, and M. Svanström, "Life cycle assessment of hydrotreated vegetable oil from rape, oil palm and Jatropha," *Journal of Cleaner Production*, vol. 19, pp. 129–137, 2011.

[29] S. Poulikidou, S. Heyne, M. Grahn, and S. Harvey, "Lifecycle energy and greenhouse gas emissions analysis of biomass-based 2-ethylhexanol as an alternative transportation fuel," *Energy Science and Engineering*, vol. 7, pp. 851–867, 2019.

[30] A. Janssen, M. Muether, A. Kolbeck, M. Lamping, and S. Pischinger, "The Impact of Different Biofuel Components in Diesel Blends on Engine Efficiency and Emission Performance," *SAE Technical Paper 2010-01-2119*, 2010.

[31] M. Johansson, J. Yang, R. Ochoterena, S. Gjirja, and I. Denbratt, "NO_x and soot emissions trends for RME, SME and PME fuels using engine and spray experiments in combination with simulations," *Fuel*, vol. 106, pp. 293–302, 2013.

[32] N. Yoshimura and M. Tamura, "Process for producing normal-octanol," p. US4417079A, 1981.

[33] T. Hamilton-Kemp, M. Newman, R. Collins, H. Elgaali, K. Yu, and D. Archbold, "Production of the long-chain alcohols octanol, decanol, and dodecanol by Escherichia coli," *Current Microbiology*, vol. 51, pp. 82–86, 2005.

[34] M. K. Akhtar, H. Dandapani, K. Thiel, and P. R. Jones, "Microbial production of 1-octanol: A naturally excreted biofuel with diesel-like properties," *Metabolic Engineering Communications*, vol. 2, pp. 1–5, 2015.

[35] J. Julis and W. Leitner, "Synthesis of 1-octanol and 1,1-dioctyl ether from biomass-derived platform chemicals," *Angewandte Chemie - International Edition*, vol. 51, pp. 8615–8619, 2012.

[36] E. J. Barrientos, J. E. Anderson, M. M. Maricq, and A. L. Boehman, "Particulate matter indices using fuel smoke point for vehicle emissions with gasoline, ethanol blends, and butanol blends," *Combustion and Flame*, vol. 167, pp. 308–319, 2016.

[37] N. Schmitz, J. Burger, E. Ströfer, and H. Hasse, "From methanol to the oxygenated diesel fuel poly(oxymethylene) dimethyl ether: An assessment of the production costs," *Fuel*, vol. 185, pp. 67–72, 2016.

[38] J. Burger, E. Ströfer, and H. Hasse, "Chemical equilibrium and reaction kinetics of the heterogeneously catalyzed formation of poly(oxymethylene) dimethyl ethers from methylal and trioxane," *Industrial and Engineering Chemistry Research*, vol. 51, pp. 12 751–12 761, 2012.

[39] P. Bokinge, S. Heyne, and S. Harvey, "Renewable OME from biomass and electricity - Evaluating carbon footprint and energy performance," *Energy Science and Engineering*, vol. 8, pp. 2587–2598, 2020.

[40] "Personal communication with Jozef Borovský, ASG Analytik-Service Gesellschaft mbH,," 2019.

[41] J. E. Dec, "A conceptual model of DI diesel combustion based on laser-sheet imaging," *SAE Technical Paper 970873*, 1997.

[42] D. L. Siebers and B. Higgins, "Flame Lift-Off on Direct-Injection Diesel Sprays Under Quiescent Conditions," *SAE Technical Paper 2001-01-0530*, 2001.

[43] S. Kook and L. M. Pickett, "Effect of fuel volatility and ignition quality on combustion and soot formation at fixed premixing conditions," *SAE Int. J. Engines 2009-01-2643*, vol. 2, pp. 11–23, 2010.

[44] R. Payri, F. J. Salvador, J. Manin, and A. Viera, "Diesel ignition delay and lift-off length through different methodologies using a multi-hole injector," *Applied Energy*, vol. 162, pp. 541–550, 2016.

[45] L. M. Pickett and D. L. Siebers, "Fuel Effects on Soot Processes of Fuel Jets at DI Diesel Conditions," *SAE Techical Paper 2003-03-3080*, 2003.

[46] J. B. Heywood, *Internal Combustion Engine Fundamentals*, 2nd ed. McGraw-Hill Education, 2018.

[47] J. M. Desantes, R. Payri, F. J. Salvador, and J. Gimeno, "Measurements of Spray Momentum for the Study of Cavitation in Diesel Injection Nozzles," *SAE Technical Paper 2003-01-0703*, 2003.

[48] Q. Wang, R. Huang, J. Ni, and Q. Chen, "Potential Improvement in PM-NO_x Trade-Off in a Compression Ignition Engine by n-Octanol Addition and Injection Pressure," *Processes*, vol. 9, 2021.

[49] H. Kosaka, T. Aizawa, and T. Kamimoto, "Two-dimensional imaging of ignition and soot formation processes in a diesel flame," *International Journal of Engine Research*, vol. 6, pp. 21–42, 2005.

[50] I. Glassman, "Soot formation in combustion processes," *22. Symposium (international) on Combustion/The Combustion Insitute*, pp. 295–311, 1988.

[51] M. Frenklach and H. Wang, "Detailed modeling of soot particle nucleation and growth," *Symposium (International) on Combustion*, vol. 23, pp. 1559–1566, 1991.

[52] K. O. Johansson, M. P. Head-Gordon, P. E. Schrader, K. R. Wilson, and H. A. Michelsen, "Resonance-stabilized hydrocarbon-radical chain reactions may explain soot inception and growth," *Science*, vol. 361, pp. 997–1000, 2018.

[53] B. Giechaskiel, J. Vanhanen, M. Väkevä, and G. Martini, "Investigation of vehicle exhaust sub-23 nm particle emissions," *Aerosol Science and Technology*, 2017.

[54] A. Ibald-Mulli, H. E. Wichmann, W. Kreyling, and A. Peters, "Epidemiological evidence on health effects of ultrafine particles," in *Journal of Aerosol Medicine: Deposition, Clearance, and Effects in the Lung*, 2002.

[55] B. Giechaskiel, R. Chirico, P. F. DeCarlo, M. Clairotte, T. Adam, G. Martini, M. F. Heringa, R. Richter, A. S. H. Prevot, U. Baltensperger, and C. Astorga, "Evaluation of the particle measurement programme (PMP) protocol to remove the vehicles' exhaust aerosol volatile phase," *Science of the Total Environment*, vol. 408, pp. 5106–5116, 2010.

[56] D. B. Kittelson, "Engines and nanoparticles: A review," *Journal of Aerosol Science*, vol. 29, pp. 575–588, 1998.

[57] L. M. Pickett and D. L. Siebers, "Soot in diesel fuel jets: effects of ambient temperature, ambient density, and injection pressure," *Combustion and Flame*, vol. 138, pp. 114–135, 2004.

[58] R. Zhang and S. Kook, "Influence of fuel injection timing and pressure on in-flame soot particles in an automotive-size diesel engine," *Environmental Science and Technology*, vol. 48, pp. 8243–8250, 2014.

[59] U. Mathis, M. Mohr, and R. Kaegl, "Influence of Diesel Engine Combustion Parameters on Primary Soot Particle Diameter," *Environmental Science & Technology*, vol. 39, pp. 1887–1892, 2005.

[60] J. M. Desantes, J. Arrègle, J. J. López, and A. García, "A comprehensive study of diesel combustion and emissions with post-injection," *SAE Technical Paper 2007-01-0915*, 2007.

[61] D. Kittelson and M. Kraft, "Particle Formation and Models in Internal Combustion Engines," in *Encyclopedia of Automotive Engineering*, 2014.

[62] J. O'Connor and M. Musculus, "Post injections for soot reduction in diesel engines: A review of current understanding," *SAE Int. J. Engines 2013-01-0917*, vol. 6, pp. 400–421, 2013.

[63] J. Martin, C. Sun, A. Boehman, and J. O'Connor, "Experimental Study of Post Injection Scheduling for Soot Reduction in a Light-Duty Turbodiesel Engine," *SAE Technical Paper 2016-01-0726*, 2016.

[64] H. Aatola, M. Larmi, T. Sarjovaara, and S. Mikkonen, "Hydrotreated Vegetable Oil (HVO) as a Renewable Diesel Fuel: Trade-off between NO_x, Particulate Emission, and Fuel Consumption of a Heavy Duty Engine," *SAE Technical Paper 2008-01-25*, 2008.

[65] K. Weidmann and H. Menrad, "Fleet Test, Performance and Emissions of Diesel Engines Using Different Alcohol-Diesel fuel Blends," *SAE Technical Paper 841331*, 1984.

[66] C. Weiskirch, M. Kaack, I. Blei, and P. Eilts, "Alternative Fuels for Alternative and Conventional Diesel Combustion Systems," *SAE Technical Paper 2008-01-2507*, 2008.

[67] J. Campos-Fernández, J. M. Arnal, J. Gomez, N. Lacalle, and M. P. Dorado, "Performance tests of a diesel engine fueled with pentanol/diesel fuel blends," *Fuel*, vol. 107, pp. 866–872, 2013.

[68] R. Swamy, T. Chandrashekar, N. Banapurmath, and S. Khandal, "Impact of Diesel-butanol Blends on Performance and Emission of Diesel Engine," *Oil and Gas Research*, pp. 1–7, 2015.

[69] D. Rakopoulos, C. Rakopoulos, R. Papagiannakis, and D. Kyritsis, "Combustion heat release analysis of ethanol or n-butanol diesel fuel blends in heavy-duty DI diesel engine," *Fuel*, vol. 90, pp. 1855–1867, 2011.

[70] B. Heuser, F. Kremer, S. Pischinger, and J. Klankermayer, "Optimization of Diesel Combustion and Emissions with Tailor-Made Fuels from Biomass," *SAE Technical paper 2013-24-0059*, 2013.

[71] A. García, J. Monsalve-Serrano, B. Heuser, M. Jakob, F. Kremer, and S. Pischinger, "Influence of fuel properties on fundamental spray characteristics and soot emissions using different tailor-made fuels from biomass," *Energy Conversion and Management*, vol. 108, pp. 243–254, 2016.

[72] B. Heuser, S. Ahling, F. Kremer, S. Pischinger, H. Rohs, B. Holderbaum, and T. Korfer, "Experimental Investigation of a RCCI Combustion Concept with In-Cylinder Blending of Gasoline and Diesel in a Light Duty Engine," *SAE Technical Paper 2015-24-2452*, 2015.

[73] T. Zhang, K. Munch, and I. Denbratt, "An Experimental Study on the Use of Butanol or Octanol Blends in a Heavy Duty Diesel Engine," *SAE Int. J. Fuels Lubr. 2015-24-2491*, vol. 8, 2015.

[74] Q. Wang, S. Yin, and J. Ni, "The effects of n-pentanol, di-n-butyl ether (DBE) and exhaust gas recirculation on performance and emissions in a compression ignition engine," *Fuel*, vol. 284, 2021.

[75] M. Pan, Z. Zheng, R. Huang, X. Zhou, H. Huang, J. Pan, and Z. Chen, "Reduction in PM and NO_x of a diesel engine integrated with n-octanol fuel addition and exhaust gas recirculation," *Energy*, vol. 187, p. 115946, 2019.

[76] B. Kerschgens, L. Cai, H. Pitsch, B. Heuser, and S. Pischinger, "Di-n-buthylether, n-octanol, and n-octane as fuel candidates for diesel engine combustion," *Combustion and Flame*, vol. 163, pp. 66–78, 2016.

[77] A. Bharti and T. Banerjee, "Reactive force field simulation studies on the combustion behavior of n -octanol," *Fuel Processing Technology*, vol. 152, pp. 132–139, 2016.

[78] J. Palmer, M. Ramesh, V. Kirsch, M. Reddemann, and R. Kneer, "Spray Analysis of C 8 H 18 O Fuel Blends using High-Speed Schlieren Imaging and Mie Scattering," *SAE Technical Paper 2015-24-2478*, 2015.

[79] T. Zhang, M. Andersson, K. Munch, and I. Denbratt, "Optical Diagnostics of Spray Characteristics and Soot Volume Fractions of n-Butanol, n-Octanol, Diesel, and Hydrotreated Vegetable Oil Blends in a Constant Volume Combustion Chamber," *SAE Technical Paper 2019-01-0019*, 2019.

[80] A. Janssen, M. Muether, S. Pischinger, A. Kolbeck, and M. Lamping, "Tailor-Made Fuels: The Potential of Oxygen Content in Fuels for Advanced Diesel Combustion Systems," *SAE Technical Paper 2009-01-2765*, 2009.

[81] P. Hottenbach, T. Brands, G. Grünefeld, A. Janssen, M. Muether, and S. Pischinger, "Optical and Thermodynamic Investigations of Reference Fuels for Future Combustion Systems," *SAE Int. J. Fuels Lubr. 2010-01-2193*, vol. 3, pp. 819–838, 2010.

[82] A. Atmanli, "Effects of a cetane improver on fuel properties and engine characteristics of a diesel engine fueled with the blends of diesel , hazelnut oil and higher carbon alcohol," *Fuel*, vol. 172, pp. 209–217, 2016.

[83] D. Rakopoulos, C. Rakopoulos, E. Kakaras, and E. Giakoumis, "Effects of ethanol–diesel fuel blends on the performance and exhaust emissions of heavy duty DI diesel engine," *Energy Conversion and Management*, vol. 49, pp. 3155–3162, 2008.

[84] S. Wang, X. Zhu, L. M. Somers, and L. P. de Goey, "Effects of exhaust gas recirculation at various loads on diesel engine performance and exhaust particle size distribution using four blends with a research octane number of 70 and diesel," *Energy Conversion and Management*, vol. 149, pp. 918–927, 2017.

[85] J. Preuss, K. Munch, and I. Denbratt, "Effect of injection strategy and EGR on particle emissions from a CI engine fueled with an oxygenated fuel blend and HVO," *SAE Technical Paper 2021-01-0560*, 2021.

[86] T. Kitamura, T. Ito, J. Senda, and H. Fujimoto, "Mechanism of Smokeless Diesel-Combustion with Oxygenated Fuels Based on the Dependence of theEquivalence Ratio and Temperature on Soot Particle Formation." *International Journal of Engine Research*, vol. 3, pp. 223–248, 2002.

[87] L. Zhou, B. Heuser, M. Boot, F. Kremer, and S. Pischinger, "Performance and Emissions of Lignin and Cellulose Based Oxygenated Fuels in a Compression-Ignition Engine," *SAE Technical Paper 2015-01-0910*, 2015.

[88] Z. Xu, X. Li, C. Guan, and Z. Huang, "Characteristics of exhaust diesel particles from different oxygenated fuels," *Energy and Fuels*, vol. 27, pp. 7579–7586, 2013.

[89] S. E. Iannuzzi, C. Barro, K. Boulouchos, and J. Burger, "POMDME-diesel blends: Evaluation of performance and exhaust emissions in a single cylinder heavy-duty diesel engine," *Fuel*, vol. 203, pp. 57–67, 2017.

[90] M. Härtl, P. Seidenspinner, E. Jacob, and G. Wachtmeister, "Oxygenate screening on a heavy-duty diesel engine and emission characteristics of highly oxygenated oxymethylene ether fuel OME1," *Fuel*, vol. 153, pp. 328–335, 2015.

[91] A. Omari, B. Heuser, and S. Pischinger, "Potential of oxymethylenether-diesel blends for ultra-low emission engines," *Fuel*, vol. 209, pp. 232–237, 2017.

[92] J. Burger, M. Siegert, E. Ströfer, and H. Hasse, "Poly (oxymethylene) dimethyl ethers as components of tailored diesel fuel : Properties , synthesis and purification concepts," *Fuel*, vol. 89, pp. 3315–3319, 2010.

[93] M. Münz, A. Mokros, D. Töpfer, and C. Beidl, "OME – Assessment of Particle Emissions in Real Driving Conditions," *MTZ worldwide*, pp. 16–21, 2018.

[94] A. Omari, B. Heuser, S. Pischinger, and C. Rüdinger, "Potential of long-chain oxymethylene ether and oxymethylene ether-diesel blends for ultra-low emission engines," *Applied Energy*, vol. 239, pp. 1242–1249, 2019.

[95] P. Dworschak, V. Berger, M. Härtl, and G. Wachtmeister, "Measurements of Neat and Water-Emulsified Oxymethylene Ethers in a Heavy-Duty Diesel Engine," *SAE Int. J. Fuels Lubr. 04-13-02-0012*, vol. 13, pp. 187–203, 2020.

[96] "ISO 5165:2017 Petroleum products — Determination of the ignition quality of diesel fuels — Cetane engine method," 2017.

[97] M. Kass, M. Wissink, C. Janke, R. Connatser, and S. Curran, "Compatibility of Elastomers with Polyoxymethylene Dimethyl Ethers and Blends with Diesel," *SAE Int. J. Adv. & Curr. Prac. in Mobility 2020-01-0620*, vol. 2, pp. 1963–1973, 2020.

[98] A. Yamaguchi, L. Koopmans, A. Helmantel, F. P. Karrholm, and P. Dahlander, "Spray Characterization of Gasoline Direct Injection Sprays under Fuel Injection Pressures up to 150 MPa with Different Nozzle Geometries," *SAE Technical Paper 2019-01-0063*, 2019.

[99] AVL List GmbH, "AVL Micro Soot Sensor: Operating Manual," List, 2013.

[100] Cambustion, "DMS500 Fast Particle Analyzer," 2018. [Online]. Available: https://www.cambustion.com/products/dms500

[101] Dekati Ltd., "Dekati ® Thermodenuder, User Manual ver 5.2," 2015.

[102] J. Sjöblom and H. Ström, "Capture of automotive particulate matter in open substrates," *Industrial and Engineering Chemistry Research*, vol. 52, pp. 8373–8385, 2013.

[103] G. Woschni, "A Universally Applicable Equation for the Instantaneous Heat Transfer Coefficient in the Internal Combustion Engine," *SAE Technical Paper 670931*, pp. 3065–3083, 1967.

[104] J. V. Brettschneider, "Berechnung des Luftverhältnisses Lambda von Luft-Kraftstoff-Gemischen und des Einflusses von Messfehlerns auf Lambda," *Bosch technische Berichte*, vol. 6, 1979.

[105] D. Bresenham, J. Reisel, and K. Neusen, "Spindt air-fuel ratio method generalization for oxygenated fuels," *SAE Technical Paper 982054*, pp. 2154–2171, 1998.

[106] C. Du, M. Andersson, and S. Andersson, "Effects of Nozzle Geometry on the Characteristics of an Evaporating Diesel Spray," *SAE Int. J. Fuels Lubr. 2016-01-2197*, vol. 9, pp. 493–513, 2016.

[107] C. Du, S. Andersson, and M. Andersson, "Two-dimensional measurements of soot in a turbulent diffusion diesel flame : the effects of injection pressure , nozzle orifice diameter , and gas density," *Combustion Science and Technology*, vol. 190, pp. 1659–1688, 2018.

[108] H. Schardin, "Die Schlierenverfahren und ihre Anwendungen," in *Ergebnisse der Exakten Naturwissenschaften*. Springer Berlin Heidelberg, 1942, pp. 303—-439.

[109] R. Ochoterena, "High Speed Shadowgraph and Diffraction Based Imaging for Spray Characterisation and Combustion Studies," *SAE Technical Paper 2009-24-0034*, 2009.

[110] J. Naber and D. L. Siebers, "Effects of Gas Density and Vaporization on Penetration and Dispersion of Diesel Sprays," *SAE Technical Paper 960034*, 1996.

[111] T. Zhang, L. Jacobson, C. Björkholtz, K. Munch, and I. Denbratt, "Effect of using butanol and octanol isomers on engine performance of steady state and cold start ability in different types of Diesel engines," *Fuel*, vol. 184, pp. 708–717, 2016.

[112] S. Shamun, M. Novakovic, V. B. Malmborg, C. Preger, M. Shen, M. E. Messing, J. Pagels, M. Tunér, and P. Tunestäl, "Detailed characterization of particulate matter in alcohol exhaust emissions," *COMODIA 2017 - 9th International Conference on Modeling and Diagnostics for Advanved Engine Systems*, 2017.

[113] "Personal communication with Dr. Nhut Lam, Test engineer at Volvo Group Trucks Technology," 2021.

[114] N. Sharma, J. Sjöblom, and J. Preuss, "Morphological Characterization of Soot from Diesel and an oxygenated fuel from a Compression Ignition Engine," *in submission*, 2021.

[115] J. Preuß, K. Munch, and I. Denbratt, "Performance and emissions of long-chain alcohols as drop-in fuels for heavy duty compression ignition engines," *Fuel*, vol. 216, pp. 890–897, 2018.

[116] P. Dworschak, V. Berger, M. Härtl, and G. Wachtmeister, "Neat Oxymethylene Ethers: Combustion Performance and Emissions of OME2, OME3, OME4 and OME5 in a Single-Cylinder Diesel Engine," *SAE Technical Paper 2020-01-0805*, 2020.

[117] P. Verma, E. Pickering, M. Jafari, Y. Guo, S. Stevanovic, J. F. Fernando, D. Golberg, P. Brooks, R. Brown, and Z. Ristovski, "Influence of fuel-oxygen content on morphology and nanostructure of soot particles," *Combustion and Flame*, vol. 205, pp. 206–219, 2019.

Abbreviations

2-EH	2-Ethylhexanol
ATDC	After top dead center
bmep	Brake mean effective pressure
CAD	Crank angle degree
CFD	Computational fluid dynamics
CFR	Cooperative Fuel Research engine
CI	Compression ignition
CN	Cetane Number
COV	Coefficient of variation
CO	Carbon monoxide
CO_2	Carbon dioxide
D	Diesel
Dec	n-Decanol
DNBE	Di-n-butyl ether
E85	Fuel containing 85 % ethanol and 15 % gasoline
EGR	Exhaust gas recirculation
FID	Flame ionisation detector
GHG	Greenhouse gas
GWP	Global warming potential
H_2O	Water
HP/HT	High-pressure/high-temperature chamber
HVO	Hydrotreated vegetable oil
ID	Ignition delay
imep	Indicated mean effective pressure
LHV	Lower heating value
MFB	Mass fraction burned
NO_x	Nitrogen oxides

Oc	n-Octanol
OH	Hydroxyl radical
OME_n	Poly(oxymethylene) dimethyl ether
PAH	Polycyclic aromatic hydrocarbons
PH	2-Propylheptanol
PM	Particle mass
PMP	Particle Measurement Programme
PN	Particle number
PSD	Particle size distribution
RED	(European) Renewable Energy Directive
RoHR	Rate of heat release
RME	Rapeseed methyl ester
SCR	Selective catalytic reaction system
SOI	Start of injection
TD	Thermodenuder
TEM	Transmission electron microscopy
UDS	Urea dosing system
UHC	unburned hydrocarbons